

8-2021

The microsatellite instability high endometrial tumor microenvironment and identifying predictive biomarkers of response to pembrolizumab

Jeffrey How

Follow this and additional works at: https://digitalcommons.library.tmc.edu/utgsbs_dissertations



Part of the [Neoplasms Commons](#)

Recommended Citation

How, Jeffrey, "The microsatellite instability high endometrial tumor microenvironment and identifying predictive biomarkers of response to pembrolizumab" (2021). *The University of Texas MD Anderson Cancer Center UTHealth Graduate School of Biomedical Sciences Dissertations and Theses (Open Access)*. 1127.

https://digitalcommons.library.tmc.edu/utgsbs_dissertations/1127

This Thesis (MS) is brought to you for free and open access by the The University of Texas MD Anderson Cancer Center UTHealth Graduate School of Biomedical Sciences at DigitalCommons@TMC. It has been accepted for inclusion in The University of Texas MD Anderson Cancer Center UTHealth Graduate School of Biomedical Sciences Dissertations and Theses (Open Access) by an authorized administrator of DigitalCommons@TMC. For more information, please contact digitalcommons@library.tmc.edu.

The microsatellite instability high endometrial tumor microenvironment and identifying
predictive biomarkers of response to pembrolizumab

by

Jeffrey Andrew How, MD, MPH

APPROVED:

Amir A. Jazaeri, MD
Advisory Professor

Greg Lizee, PhD

Aung Naing, MD

Linghua Wang, MD, PhD

Melinda S. Yates, PhD

APPROVED:

Dean, The University of Texas
MD Anderson Cancer Center UTHealth Graduate School of Biomedical Sciences

The microsatellite instability high endometrial tumor microenvironment and identifying
predictive biomarkers of response to pembrolizumab

A

Thesis

Presented to the Faculty of

The University of Texas

MD Anderson Cancer Center UTHealth

Graduate School of Biomedical Sciences

in Partial Fulfillment

of the Requirements

for the Degree of

Master of Science

by

Jeffrey Andrew How, MD, MPH

Houston, Texas

August 2021

Copyright

by

Jeffrey Andrew How, MD, MPH

2021

Acknowledgements

First, I would like to thank my parents, Redge and Florence, for all their support and encouragement throughout the years; I would not be where I am or achieve all that I have without you both.

Thank you, Dr. Amir Jazaeri, for all your mentorship, guidance, and patience. Your passion for science is contagious and have helped to enhance my critical thinking and problem solving skills. you are a role model for the type of translational researcher I would like to become in the future. Under your mentorship, these past two years have been a very rewarding experience and I truly thank you for all the opportunities.

I am grateful for Drs. Linghua Wang and Minghao Dang for their integral involvement in this project and bioinformatics expertise that helped to make this project a reality. Thank you to Dr. Elizabeth Euscher and Joseph Celestino who aided to help procure key tumor samples for this project.

Lastly, thank you to all members of the MS thesis committee who have provided valuable feedback to improve the quality of this project.

This project was supported in part by the National Institute of Health T32 training grant (T32 CA101642) and the uterine SPORE grant (CA098258).

The microsatellite instability high endometrial tumor microenvironment and identifying
predictive biomarkers of response to pembrolizumab

Jeffrey Andrew How, MD, MPH

Advisory Professor: Amir A. Jazaeri, MD

Abstract

Objective: Half of patients with microsatellite instability high (MSI-H) endometrial cancer are treatment-refractory to pembrolizumab. We sought to evaluate the MSI-H endometrial tumor samples to examine differences in the tumor microenvironment (TME) and identify transcriptomic signatures associated with response/resistance to pembrolizumab.

Methods: Archival tumor samples from MSI-H endometrial cancer patients treated at MD Anderson Cancer Center were obtained. Tissue samples originating from patients who did not receive pembrolizumab treatment (“untreated cohort”; n = 11) were analyzed via RNA sequencing (RNA-seq). Pre-treatment archival tumor samples (“treated cohort”; n = 23) from patients who were later treated with pembrolizumab were collected and analyzed by Exome Capture RNA-seq to identify predictive immuno-genomic signatures associated with treatment response. Multipanel immunofluorescent panel testing was performed on samples in the treated cohort.

Results: In the untreated cohort (n=11), the transcriptomic profiles of the samples could be segregated into three subcategories. Four samples were immunologically “hot” as evidenced by an abundance of pro-inflammatory immune cell infiltrate, 3 had a paucity of this infiltrate (“cold”), and 4 samples had intermediate amounts (“warm”). In the treated cohort (n=23), the transcriptomic profiles could similarly be subdivided into

three subcategories. The 14 responders consisted of samples with “hot” (5/5; 100%), “cold” (6/8; 75%), and “warm” TMEs (3/8; 37.5%) while the 7 non-responders consisted of only “cold” (2/8; 25%) and “warm” (5/8; 62.5%) TME samples. Two patients had an unevaluable response to pembrolizumab. We observed an enrichment of fibroblasts and endothelial cell transcriptomic signatures in the samples of the non-responders compared to responders ($p = 0.018$). Additionally, there was an inverse relationship between enrichment of fibroblast and endothelial cell transcriptomic signatures and strength of treatment response. Responders had higher total ($p = 0.029$) and PD-L1⁺ macrophage ($p = 0.012$) cell densities compared to non-responders.

Conclusions: TME composition appears to be heterogeneous among MSI-H endometrial tumors. Decreased macrophages and increased presence of fibroblasts and endothelial cells in the TME may contribute to innate resistance to pembrolizumab. Adjunctive therapy that optimizes these cellular subpopulations may help overcome pembrolizumab resistance. Future studies are needed to validate these findings

Table of Contents

Approval Sheet:.....	i
Title Page.....	ii
Copyright.....	iii
Acknowledgements.....	iv
Abstract.....	v
List of Figures	ix
List of Tables	x
List of abbreviations.....	xi
Introduction	1
Overview	1
Molecular classification of endometrial cancer	3
Immune checkpoint inhibitors in endometrial cancer.....	5
Innate resistance to PD-1 inhibitors.....	6
Hypothesis and Specific Aims	11
Materials and Methods.....	12
Tumor specimen identification and clinical data retrieval	12
RNA extraction	13
Fresh frozen samples.....	13

FFPE samples	14
RNA sequencing	16
Multiplex immunofluorescence	19
Statistical analysis.....	22
Results	24
Clinicopathologic characteristics.....	24
MSI-H endometrial TMEs display a diversity of immune cell subpopulations	29
Transcriptomic signatures in the TME shape response to pembrolizumab	31
Endothelial cells and fibroblasts in the TME are associated with poor response to pembrolizumab	33
Differential gene expression tumors with endothelial cell and fibroblast enrichment in the TME.....	38
TME is a prognostic biomarker for survival following pembrolizumab therapy	41
PD-L1/PD-1/TIL mIF testing	45
Discussion.....	56
Conclusions	62
Bibliography	63
Vita	81

List of Figures

Figure 1 - Segregation of MSI-H endometrial tumors into "hot" and "cold" subtypes	9
Figure 2 - Molecular features of MSI-H "hot" and "cold" subtypes	10
Figure 3 - Progression-free survival by response to pembrolizumab	28
Figure 4 - Overall survival by response to pembrolizumab	29
Figure 5 - Transcriptomic profile of untreated cohort of MSI-H endometrial tumors.....	30
Figure 6 - Transcriptomic profile of MSI-H endometrial tumors in the treated cohort...	31
Figure 7 - Response to pembrolizumab based on tumor microenvironment.....	33
Figure 8 - Endothelial cell and fibroblast marker gene expression.....	35
Figure 9 - Endothelial cell and fibroblast marker gene expression by response type...	36
Figure 10 - Immune cell subpopulation and response to pembrolizumab	38
Figure 11 - Differential gene expression based on fibroblastic status.....	40
Figure 12 - Progression-free survival based on tumor microenvironment subtype and fibroblastic group status	43
Figure 13 - Overall survival based on tumor microenvironment subtype and fibroblastic group status	45
Figure 14 - T lymphocytes by tumor microenvironment subtype.....	47
Figure 15 - T lymphocytes by response	50
Figure 16 - Macrophages population by tumor microenvironment	53
Figure 17 - Macrophage population by response.....	54
Figure 18 - PD-L1 positivity in tumor cells.....	55

List of Tables

Table 1 - 5 year survival of uterine cancer based on FIGO stage at diagnosis (9)	2
Table 2 - Multiplex immunofluorescent panel.....	19
Table 3 - Clinicopathologic characteristics of the untreated cohort.....	24
Table 4 - Clinicopathologic characteristics of the treated cohort.....	25

List of abbreviations

α -SMA	Alpha-smooth muscle actin
BMI	Body mass index
cDNA	Complementary DNA
CI	Confidence interval
CR	Complete response
CXCL9	Chemokine (C-X-C) motif ligand 9
dMMR	Mismatch repair deficient
EC-RNA-seq	Exome capture RNA sequencing
FAP	Fibroblast activation protein
FFPE	Formalin-fixed paraffin embedded
H&E	Hematoxylin & eosin
IFN- γ	Interferon gamma
IHC	Immunohistochemistry
MDSC	Myeloid-derived suppressor cells
MHC	Major histocompatibility complex
mIF	Multiplex immunofluorescent
MMR	Mismatch repair
mRNA	Messenger RNA
MSI	Microsatellite instability
MSI-H	Microsatellite instability high
MSS	Microsatellite stable
NGS	Next-generation sequencing
NK cells	Natural killer cells

NOS	Not otherwise specified
OR	Odds ratio
ORR	Objective response rate
PD	Disease progression
PD-1	Programmed cell death protein 1
PD-L1	Programmed cell death-ligand 1
pMMR	Proficient mismatch repair
POLE	Polymerase ϵ
PR	Partial response
PTEN	Phosphatase and tensin homolog
qPCR	quantitative polymerase chain reaction
RNA-seq	RNA sequencing
TAM	Tumor-associated macrophages
TCGA	The Cancer Genome Atlas
TGF- β	Transforming growth factor beta
Thy-1	Thymocyte differentiation antigen 1
TIL	Tumor infiltrating lymphocytes
TMB	Tumor mutational burden
TME	Tumor microenvironment
Treg	Regulatory T cells
VEGF	Vascular endothelial growth factor

Introduction

Overview

Endometrial cancer is the most common gynecologic malignancy in the United States and it is estimated that 66,570 new cases will be diagnosed and 12,940 deaths will occur annually [1]. Historically, endometrial cancer has been classified into two broad histopathologic categories: type I (endometrioid) or II (non-endometrioid) [2]. These two categories differ in epidemiologic risk factors and clinical behavior [2, 3]. Type I tumors comprise the majority (80 – 90%) of endometrial cancers and are associated with factors that promote states of unopposed estrogen excess (e.g. estrogen without progesterone) [2-5]. These risk factors include but are not limited to obesity, diabetes mellitus, polycystic ovarian syndrome, early menarche, late menopause, nulliparity, and tamoxifen therapy [6-8]. Type II tumors comprise 10 – 20% of endometrial cancers and consist of serous, clear cell, carcinosarcoma, mucinous, squamous, transitional cell, mesospheric, and undifferentiated histologies [2, 3]. Relative to those with type I endometrial cancers, patients with type II endometrial cancer are more likely to be older, normal body mass index (BMI), and non-White race [3, 6]. Furthermore, type II endometrial cancers tend to have worse prognosis [4]. Obesity is a modifiable risk factor that is strongly associated with endometrial cancer with increasing BMI resulting in higher risk of type I endometrial cancer (OR 1.5 – 7.1 for BMI ≥ 25 kg/m²) and to a lesser extent type II endometrial cancer (OR 1.2 – 3.1 for BMI ≥ 25 kg/m²) [6]. Thus, as obesity rates continue to rise in the United States, the rates of endometrial cancer will continue to rise and become more widespread and an increasing public health issue [1, 4, 7].

The most common symptom of endometrial cancer is postmenopausal bleeding and thus many patients will be diagnosed with early stage disease, that is disease confined to the uterus. Given that most endometrial cancers will present at early stage, surgical management with total hysterectomy, bilateral salpingo-oophorectomy, and lymph node sampling with or without postoperative adjuvant radiation therapy will be curative. Despite the favorable prognosis of early stage endometrial cancer, advanced stage disease portends poor prognosis (**Table 1**) [9].

Table 1 - 5 year survival of uterine cancer based on FIGO stage at diagnosis [9]

Stage	Disease location	5-year survival
IA	Confined to uterus: less than 50% myometrial invasion	89.6%
IB	Confined to uterus: greater than 50% myometrial invasion	77.6%
II	Cervical stromal invasion	73.5%
IIIA	Involvement of uterine serosa or adnexae	56.3%
IIIB	Involvement of vagina or parametria	36.2%
IIIC1	Involvement of pelvic lymph nodes	57.0%
IIIC2	Involvement of para-aortic lymph nodes	49.4%
IVA	Involvement of bowel or bladder	22.0%
IVB	Distant metastasis	21.1%

Additionally, advanced or recurrent endometrial cancers are challenging to treat with worsening response rates to increasing lines of conventional therapy [10, 11].

Despite heterogeneity in histopathologic characteristics and disease biology among endometrial tumors, patients presenting with non-resectable advanced stage or relapse are homogenously treated with platinum-based chemotherapy regimens (e.g. carboplatin and paclitaxel) [10, 11]. Once platinum-based chemotherapy fails, subsequent therapies are observed to have modest response rates (9.5 – 24.5%) with worsening responses as the number of prior systemic therapies increases [10-15]. Despite overall poor prognosis for advanced or recurrent endometrial cancer, focusing on molecular features of endometrial cancer may better tailor management and selection of conventional and newer therapies to optimally provide clinical benefit [4].

Molecular classification of endometrial cancer

A joint effort by the National Cancer Institute and National Human Genome Research Institute that began in 2006, the Cancer Genome Atlas (TCGA) is a landmark cancer genomics program that has molecularly characterized multiple cancer types and has generated immense amount of publicly available genomic, epigenomic, transcriptomic, and proteomic data. For endometrial cancer, 373 endometrial tumors (primarily endometrioid and serous histologies) were characterized using array- and sequencing-based technologies [16]. In the TCGA analysis, endometrial tumors were broadly classified into 4 categories: polymerase ϵ (POLE) ultramutated, microsatellite instability (MSI) hypermutated, copy-number low, and copy-number high [16]. As its name suggests, the POLE hypermutated group is associated with the highest number of mutations [16]. The copy-number high group represents serous-like tumors and has a low mutation rate. The copy-number low group represents the majority of endometrial tumors characterized in the TCGA and are composed of microsatellite stable (MSS) tumors. The MSI group in the TCGA analysis is characterized by tumors with high

levels of microsatellite instability (MSI-H) with a high number of mutations and are predominantly of endometrioid histology [16]. Microsatellites are repeated segments of DNA with a propensity for replication errors; these errors are typically corrected by DNA mismatch repair (MMR) proteins [17]. Dysfunction in the MMR machinery will result in high levels of microsatellite instability. The cause of MMR function loss in endometrial tumors is typically due to sporadic methylation of the MLH promotor and is less frequently due to germline mutations (e.g. MLH1, MSH2, MSH6, or PMS2 mutations in Lynch syndrome) [18, 19].

Conventional histopathologic classification has resulted in inter-observer heterogeneity and thus the molecular categorization of endometrial cancers offers a more precise and refined approach to classification [16]. Furthermore, these categories carry differing prognostic information and response to treatment [4, 16, 20, 21]. Although representing the smallest proportion of tumors, the POLE group is associated with the best progression-free survival (PFS) and is followed by the MSI, copy-number low, and copy-number high groups [16, 20]. A retrospective analysis of the PORTEC-3 clinical trial demonstrated that certain adjuvant therapy approaches may be advantageous for certain molecular categories. For example, POLE mutant tumors had excellent PFS regardless of the adjuvant treatment arm (chemoradiation vs radiation only) and may be spared adjuvant chemoradiation [21]. On the other hand, tumors with abnormal P53 mutations (corresponding to the copy-number high category) had improved PFS with chemoradiation and thus may benefit from this strategy [21]. More recently, immunotherapy has become an advantageous and favorable treatment alternative for solid tumors. Particularly, MSI status is an important biomarker of response to immune checkpoint inhibitor therapy [22].

Immune checkpoint inhibitors in endometrial cancer

Essential to protect the human body against foreign pathogens, the immune system also plays an integral role in eliminating cancerous cells at various checkpoints throughout the process of immune surveillance [23]. Malignant cells may evade these normal immune checkpoints by several mechanisms, including programmed cell death protein-1 (PD-1) and programmed cell death ligand (PD-L1), which serve to down-regulate T-cell activity and thus favor tolerance and tumor growth [24, 25].

Immunotherapy treatments seek to elicit and/or boost the human body's natural antitumor immune response [26, 27]. The first efficacy of immune checkpoint inhibitors in MSI-H/mismatch repair deficient (dMMR) tumors was demonstrated in a landmark phase II trial by Le and colleagues [28]. In this trial, dMMR and MMR-proficient (pMMR) colorectal cancers and other dMMR solid tumors treated with pembrolizumab (anti-PD-1 antibody), patients with dMMR cancers had clinically significant objective response rates (ORR) of 30-70% and an improved PFS. Among colorectal cancer patients, those with pMMR tumors demonstrated no responses [28]. Similarly, the benefit of pembrolizumab was observed in other non-colorectal MSI-H/dMMR tumors [29]. In KEYNOTE-158, pembrolizumab demonstrated impressive responses in the endometrial cancer cohort [29]. In a cohort of 49 evaluable MSI-H endometrial cancer patients, the ORR was 57.1% with 20 partial and 8 complete responses [29]. Additionally, the median PFS and overall survival (OS) was 25.2 months (95% CI 4.9 to not reached) and not reached (95% CI 27.2 to not reached) [29]. Furthermore, the median duration of response was not reached (95% CI 2.9 to 27+ months) [29]. These are remarkable responses given that pembrolizumab monotherapy in MSS endometrial tumors has an ORR of 13% [30]. Given the clinical benefit, pembrolizumab was given

accelerated United States Food and Drug Administration (FDA) approval for use in unresectable or metastatic MSI-H/dMMR solid tumors that have progressed on prior systemic therapy in May 2017. This accelerated approval represents the first tissue agnostic indication for a drug. Since pembrolizumab's accelerated approval, other trials have demonstrated efficacy with other PD-1 (nivolumab and dostarlimab) and PD-L1 (avelumab and durvalumab) inhibitors in MSI-H/dMMR endometrial tumors [31-34]. Despite efficacy of pembrolizumab, approximately half of patients will not respond to treatment and it is unclear which patients will respond [29]. Furthermore, optimally selecting patients who will respond to pembrolizumab is critical given the potential risk of life-threatening immune-related side effects that can occur with therapy [35]. Potential mechanisms of resistance to PD-1 inhibitors will be discussed below.

Innate resistance to PD-1 inhibitors

Resistance to PD-1 inhibitor therapy in solid tumors can be broadly classified into either innate or adaptive resistance. In the latter, therapeutic resistance develops after an initial anti-tumor response and mechanisms include but are not limited to loss of T cell effector function, disruption of antigen presentation, and acquired interferon resistance [36-40]. For innate resistance, there is an absence of anti-tumor response and this may be due to several potential mechanisms.

Tumor somatic mutations in several signaling pathways have been associated with T cell exclusion from the tumor microenvironment (TME) [40]. Increased β -catenin/Wnt pathway signaling is associated with a reduction of CD8⁺ T cell and CD103⁺ dendritic cell infiltration into the TME [40, 41]. Mutations resulting in overactivation of the mitogen activated protein kinase (MAPK) signaling pathway and subsequent production of vascular endothelial growth factor (VEGF) have also been

associated with reduced T cell infiltration and PD-1 inhibitor resistance [42, 43]. The loss of phosphatase and tensin homolog (PTEN) function, a negative regulator of the PI3K pathway, is a common mutation in endometrial tumors and is associated with increased VEGF production and reduced T cell infiltration is [16, 40, 44].

Another mechanism of innate resistance to PD-1 inhibitors is failure of effective interferon-gamma (IFN- γ) signaling. Following recognition of the neoantigen peptides from the tumor cell, CD8⁺ T cells typically produce IFN- γ which result in downstream JAK1/2 activation, subsequent STAT1 and STAT3 recruitment/phosphorylation, and ultimately interferon regulatory factor activation [40, 45-47]. The increased activity of interferon regulatory factor results in downstream transcriptional activity to produce anti-tumor effects (improved recognition of tumor neoantigens, T cell infiltration, and cytotoxic T cell mediated tumor destruction) [40, 45-47]. Thus, mutations in this pathway (e.g. JAK1/2 loss of function mutations or STAT1/3 down regulation) can result in an impaired anti-tumor response in CD8⁺ cells despite PD-1 inhibition [40, 48, 49].

Another mechanism of primary resistance is poor tumor immunogenicity resulting in low concentrations of tumor infiltrating lymphocytes (TIL) [40]. Poor tumor immunogenicity may occur due to mechanisms that disrupt the major histocompatibility complex (MHC) – antigen presentation process that is essential for neoantigen peptide recognition and subsequent T cell activation/recruitment [50, 51]. Low neoantigen load is another contributing cause to lower tumor immunogenicity and also increases the likelihood of PD-1 inhibitor resistance [52]. This mechanism of resistance may help to explain the poorer responses of PD-1 inhibitors in MSS tumors as these tumors typically have lower neoantigen loads compared to MSI-H tumors [52]. Tumor

mutational burden (TMB) is defined as the total number of somatic mutations per coding area of the tumor genome and serves as a surrogate for neoantigen load as higher mutational load correlates with higher neoantigens produced [53]. Thus, tumors with lower TMB are less likely to respond to PD-1 inhibitors [54, 55]. Interestingly, in a study by Valero and colleagues, they retrospectively evaluated cohort of multiple MSS solid tumor types who were treated with PD-1 or PD-L1 inhibitors [55]. They found that those with high TMB (cutoff 10 mutations/megabase) were more likely to respond to immune checkpoint inhibitors than those with low TMB [55].

Lastly, increased presence of immunosuppressive cells in the tumor microenvironment may result in innate resistance to PD-1 inhibitors. Type II tumor-associated macrophages (TAM) are associated with pro-tumorigenesis as they produce immunosuppressive cytokines such as VEGF, MMP-9, and uPA [56, 57]. Additionally, myeloid-derived suppressor cells (MDSC) are a heterogeneous group of immature myeloid cells that typically have immunosuppressive effects in the TME [58-60]. MDSCs exert their immunosuppressive in the TME by inhibition of cytotoxic T cells via local nutrient depletion, free radical production, and induction of regulatory T cells (Treg) [58-60]. These factors serve to increase immune tolerance and promote PD-1 inhibitor resistance [40, 58].

Although there are many published studies on innate PD-1 inhibitor resistance in other solid tumors, there are relatively few studies published evaluating resistance mechanisms in endometrial cancer, let alone MSI-H endometrial tumors. Prior studies evaluating potential biomarkers of response for PD-1 inhibitors in endometrial cancer have been limited and have focused mainly on concentrations of tumor-infiltrating lymphocytes and PD-L1 positivity [30, 61]. Searching for alternative immuno-genomic

biomarkers, the group at MD Anderson Cancer Center led by Dr. Linghua Wang et al. evaluated transcriptomic profiles of PD-1 inhibitor naïve MSI-H endometrial tumor samples in the TCGA dataset. In this unpublished data, they identified two types of MSI-H endometrial TMEs. In the “hot” subtype, the TME had a significant infiltration of anti-tumor immune cells while the “cold” subtype had a paucity of such cells (**Figure 1**).

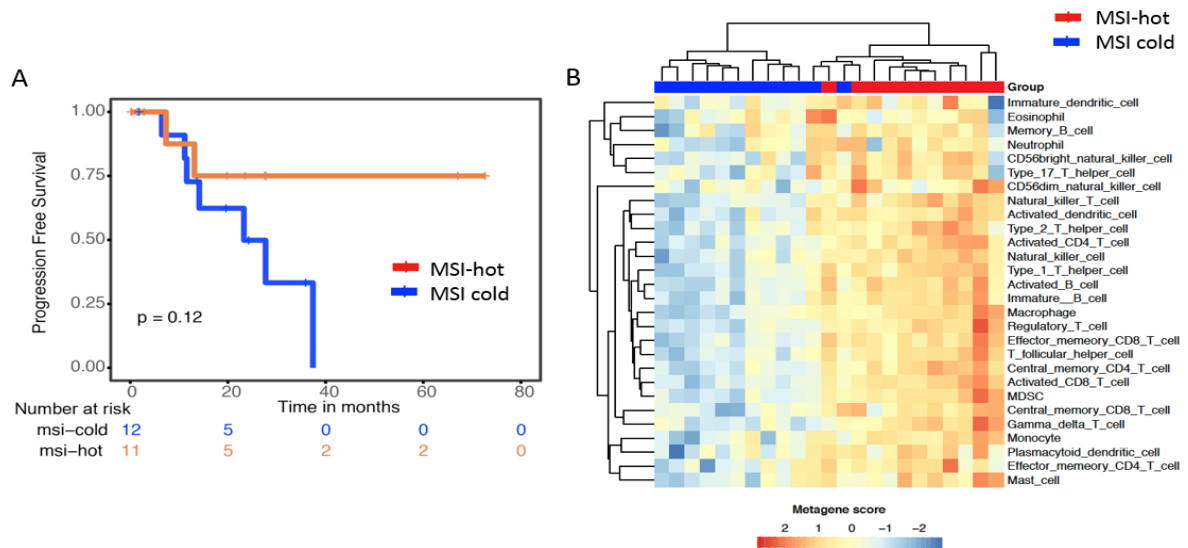


Figure 1 - Segregation of MSI-H endometrial tumors into "hot" and "cold" subtypes. A. MSI-H hot tumors demonstrated a trend toward better progression-free survival. B. MSI-hot tumors are associated with higher expression of gene signatures involved in a number of immunologic pathways. Figure used with permission by Dr. Linghua Wang et al. (unpublished work)

Furthermore, there was a trend in prognostic differences between the “hot” and “cold” groups with better PFS in the “hot” group (**Figure 1**). Neoantigen load was observed to be similar in the “hot” and “cold” groups (**Figure 2**), suggesting other factors contributing to anti-tumor immune cell recruitment and potentially PD-1 inhibitor response.

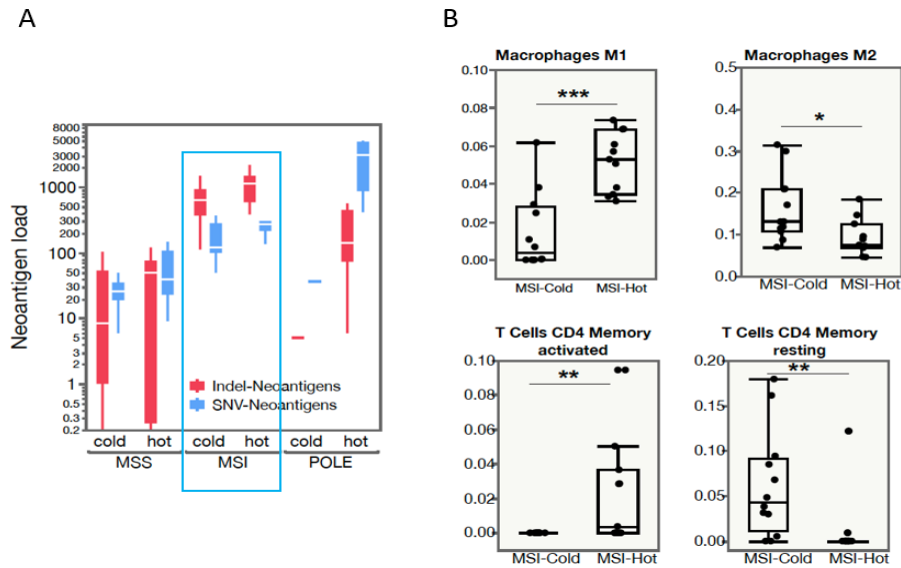


Figure 2 - Molecular features of MSI-H "hot" and "cold" subtypes

A. Genomic alterations and associated predicted neoantigen load in hot and cold subsets of different molecular subtypes of endometrial cancers.

B. Differential expression of macrophage and CD4 T_{memory} signatures in hot and cold tumors.

MSS: microsatellite stable; MSI: microsatellite instable; POLE: DNA polymerase ϵ mutated

Figure used with permission by Dr. Linghua Wang et al (unpublished work)

Further comprehension of the MSI-H endometrial tumors and their impact on the TME are critical to elucidating mechanisms of innate resistance to pembrolizumab. These TME subtypes highlight the possibility that an immunosuppressive TME is responsible for innate resistance to pembrolizumab. Thus in this thesis, the objective is to identify resistance pathways to pembrolizumab in MSI-H endometrial cancer by evaluating the TME.

Hypothesis and Specific Aims

Central Hypothesis: “Cold” TMEs associated with immune cell exclusion will be correlated with increased resistance to pembrolizumab in patients with MSI-H endometrial cancer.

Specific Aim 1: Characterize the diversity of MSI-H endometrial tumors through analysis of immune and non-immune cell subpopulations in the TME using RNA sequencing.

Specific Aim 2: Characterize transcriptomic signals in the MSI-H endometrial TME and determine their association with response to pembrolizumab.

Materials and Methods

Tumor specimen identification and clinical data retrieval

For this retrospective single-institution study at the University of Texas MD Anderson Cancer Center, tumor samples of patients with MSI-H endometrial cancer were identified and collected under an Institutional Review Board protocol (PA19-0725). Tumor samples were identified via several methods. For Specific Aim 1, available fresh frozen tumor samples were collected from the MD Anderson Department of Gynecologic Oncology and Reproductive Medicine tumor bank. These tumor samples consisted of tumor specimens from the initial surgical staging procedure as part of their surgical management of early stage disease that was performed at MD Anderson. Additionally, these tumor samples were from patients who were not treated with pembrolizumab (“untreated” cohort). For Specific Aim 2, tumor samples were obtained from patients who were treated with pembrolizumab after May 2017 (“treated” cohort). All samples were formalin-fixed paraffin embedded (FFPE) tumor samples that were obtained in the primary and/or recurrent setting. Of note, all the FFPE tumor samples were all samples prior to pembrolizumab treatment. In the treated cohort, patients were identified utilizing an electronic medical record database search of endometrial cancer patients who were treated with pembrolizumab in clinical practice at MD Anderson from May 2017 to November 2019. In collaboration with a gynecologic oncology pathologist, additional patients were identified through a query of the institutional pathology database to identify endometrial tumors with MSI-H status.

Once a list of potential patients and samples were obtained for inclusion into the study, confirmation of MSI-H status for the untreated and treated cohorts were performed through medical chart review. MSI-H status was determined through

immunohistochemistry (IHC) staining with loss of MMR proteins (MLH1, MSH2, MSH6, and/or PMS2) and/or polymerase chain reaction (PCR) for methylation of the MLH1 promoter and microsatellite marker panel testing [62, 63]. For the list of potential patients in the treated cohort, pembrolizumab administration (whether at MD Anderson or an outside hospital) was confirmed through medical chart review.

Clinical data was extracted from the electronic medical records. Collected demographic and clinicopathologic information included the following: age, BMI, tumor histology, tumor grade, cause of MSI-H, initial stage, comorbidities, and prior treatment history. Extracted pembrolizumab treatment information included the following: dates of pembrolizumab initiation and completion, number of treatment cycles, treatment response, date of disease progression, date of death, and date of last follow-up.

RNA extraction

Fresh frozen samples

For the fresh frozen samples of the untreated cohort, the following procedure was performed for RNA extraction at the MD Anderson Biospecimen Extraction facility using the RNeasy mini Kit (Qiagen, Hilden, Germany) according to the manufacturer's protocol, as excerpted below:

- 1) Tissue disruption and homogenization of the lysate in 350 μ l of Buffer RLT (10 ml of β -Mercaptoethanol per 1 ml Buffer RLT)
- 2) Centrifugation of the lysate for 3 minutes at full speed followed by transfer of supernatant to a new microcentrifuge tube
- 3) On the supernatant, 70% ethanol was added and mixed by pipetting. Up to 700 μ l of the mixed sample was transferred to a 2 ml collection tube and

placed in an RNeasy spin column followed by centrifugation for 15 seconds at $\geq 8000 \times g$. The flow was discarded.

- 4) 700 μ l of Buffer W1 was added to the RNeasy spin column followed by centrifugation for 15 seconds at $\geq 8000 \times g$. The flow was discarded.
- 5) 500 μ l of Buffer RPE was added to the RNeasy spin column followed by centrifugation for 15 seconds at $\geq 8000 \times g$. The flow was discarded.
- 6) 500 μ l of Buffer RPE was added to the RNeasy spin column followed by centrifugation for 2 minutes at $\geq 8000 \times g$. The flow was discarded.
- 7) The RNeasy spin column is placed in a new 1.5 ml collection tube and 30 – 50 μ l of RNase-free water is added directly to the spin column membrane and centrifuged for 1 minute at $\geq 8000 \times g$.
- 8) The extracted RNA is stored at -80 C until submission for RNA sequencing (RNA-seq)

FFPE samples

Once the FFPE samples were collected, one 5 μ m section was stained with haematoxylin & eosin (H&E) and the region and percentage of tumor in section was demarcated by a collaborating gynecologic oncology pathologist. At the MD Anderson Biospecimen Extraction Facility, RNA extraction was performed on three to five 5 μ m sections using the High Pure FFPE RNA isolation kit (Roche, Basel, Switzerland) in accordance with the manufacturer's protocol, as excerpted below.

Each unstained FFPE section underwent deparaffinization as follows:

- 1) 800 μ l of xylene was added and vortexed at several intervals

- 2) 400 μ l of absolute ethanol was added and vortexed briefly. Centrifugation for 2 minutes at maximum speed (16,000 x g) and supernatant discarded
- 3) 1 ml of absolute ethanol added and vortexed briefly. Centrifugation for 2 minutes at maximum speed (16,000 x g) and supernatant discarded
- 4) Tissue pellet dried for 10 minutes at 55 C

Following deparaffinization, RNA isolation was performed as follows:

- 1) 100 μ l RNA Tissue Lysis buffer, 16 μ l 10% SDS, and 40 μ l Proteinase K working solution added to tissue pellet and vortexed for several seconds followed by 30 minute incubation at 85 C with shaking at 600 revolutions per minute (rpm) and spun down briefly and cooled to <55 C
- 2) 80 μ l of Proteinase K was added and vortexed for several seconds followed by incubation at 30 minutes and with shaking at 600 rpm and spun down briefly. If lysate was not clear then incubation was extended another 10 minutes
- 3) 325 μ l of RNA Binding buffer and μ l of absolute ethanol was added and vortexed for several seconds then spun down briefly
- 4) The tissue lysate was pipet into the upper reservoir of a High Pure Filter Tube assembly followed by centrifugation at 6000 x g for 30 seconds. The High Pure Filter Tube was placed onto a new High Pure Collection Tube and centrifuged for 16,000 x g to dry the filter fleece completely.
- 5) The High Pure Filter tube was placed onto a new High Pure Collection Tube and 100 μ l of DNase working solution was added onto the High Pure Filter Tube Fleece followed by incubation between 15 – 25 C for 15 minutes
- 6) 500 μ l of Wash Buffer I working solution was added followed by centrifugation at 6,000 x g for 20 seconds and the flow was discarded. This step was repeated.

- 7) Centrifugation was repeated for 2 minutes at 16,000 x g to dry the filter fleece completely. The High Pure Filter Tube was placed into a fresh 1.5 ml reaction tube.
- 8) 25 – 50 µl of RNA Elution Buffer was added to the center of the fleece tube and incubated for 1 minute at 15 – 25 C followed by centrifugation for 1 minute at 6,000 x g.
- 9) The eluted RNA was stored at -80 C until submission for RNA sequencing (RNA-seq)

RNA sequencing

RNA-seq was performed on at least 100 – 200 ng of extracted RNA per sample from both the untreated and treated cohorts at the MD Anderson Advanced Technology Genomics Core (ATGC) facility. For the untreated cohort, TruSeq Stranded Total RNA library prep kit (Illumina, San Diego, CA) was utilized according to the manufacturer's protocol in order to convert the extracted RNA into libraries for sequencing. In brief, ribosomal RNA was removed from the total RNA using biotinylated, target-specific oligos combined with ribosomal RNA removal beads and underwent subsequent RNA fragmentation using divalent cations. These RNA fragments underwent conversion into double-stranded complementary DNA (cDNA) fragments using reverse transcriptase and random primers for the first cDNA strand and DNA polymerase I and RNase H for the second cDNA strand. The 3' ends of the blunt fragments were adenylated with a single 'A' nucleotide to prevent ligation. Following conversion, library preparation was performed. The cDNA fragments were ligated to specific sequencing adapters of appropriate size and DNA fragments were enriched using PCR for 12 cycles. Once the sequencing library was completed, the library is quantified by quantitative PCR and

checked for quality using the Agilent 4200 TapeStation System with the Agilent High sensitivity D1000 ScreenTape Assay (Agilent technologies, Santa Clara, CA). Following the quality check, Illumina next-generation sequencing (NGS) using HiSeq4000 system was performed in two lanes with a 76 nt paired-end sequencing format.

For the extracted RNA from the treated cohort, Exome Capture RNA-seq (EC-RNA-seq) was performed given the RNA from FFPE tissue is frequently degraded and more prone to failure utilizing traditional RNA-seq technology. For the treated cohort, TruSeq RNA Exome library prep kit (Illumina, San Diego, CA) was utilized according to the manufacturer's protocol in order to convert the extracted RNA into libraries for sequencing. In brief, RNA was fragmented and primed cDNA synthesis. Following cDNA synthesis of both strands, the 3' ends were adenylated with a single 'A' nucleotide and the cDNA fragments were ligated to specific adapters; these fragments were subsequently enriched. Next, pre-amplification library quantification and quality check was performed using the Agilent 4200 TapeStation System with the Agilent High sensitivity D1000 ScreenTape Assay. Following quality check, DNA libraries were pooled together and capture probes were used to target specific regions of DNA of interest. Streptavidin magnetic beads were then used to capture hybridized probes and two heated washes remove nonspecific bead binding. Second hybridization was performed to improve specificity of captured regions. AmPure XP beads were used to purify the enriched captured library prior to amplification by PCR. This protocol captured 214,126 targets spanning 21,425 genes covering 98.3% of the RefSeq Exome. The enriched library was amplified by PCR for 10 cycles followed by purification with AmPure XP beads. Quality check was subsequently performed using

the Agilent 4200 TapeStation System with the Agilent High sensitivity D1000 ScreenTape Assay. Following RNA-seq and EC-RNA-seq completion, the raw data was submitted to the MD Anderson Computational Biology Lab for bioinformatics analysis.

Bioinformatics analysis

Bioinformatics analyses for RNA-seq quality control, identification of differentially expressed genes, and hierarchal clustering was performed as previously described [64]. Quality control of the generated RNA-seq data was performed via FastQC (v0.11.5) and RNA-seQC; all samples passed the quality check [65, 66]. Following quality control measures, RNA-seq BAM files were generated using STAR 2-pass alignment on default parameters[67]. From these RNA-seq BAM files, gene expression values were generated for purposes of identifying differentially expressed genes and performing hierarchal clustering. First, the HTSeq was tool utilized on these BAM files to generate a count of reads mapped to each gene [68]. These counts were subsequently processed by the Deseq2 software (v3.6) in order to identify differential expression of genes across samples [68, 69]. The most differentially expressed genes were defined by a gene expression fold change threshold of ≥ 2 or ≤ -0.5 and a false discovery rate q-value ≤ 0.01 . For hierarchal clustering, analyses followed the RNA quantification approach recommended by the bioinformatics team of the National Cancer Institute Genomics Data Commons [64, 70, 71]. This approach consisted of normalizing counts generated from HTSeq into fragments per kilobase of transcript per million (FPKM) demonstrated by the following equation [64, 70]:

$$FPKM = \frac{RCg * 10^9}{RCpc * L}$$

In this equation, RC_g refers number of reads mapped to a gene, RC_{pc} refers to the number of reads mapped to all genes encoding proteins and L refers to the length of genes in base-pairs [64, 70, 71]. These FPKM were subsequently log2-transformed and inputted into the MCPcounter, an R statistical package that utilizes the Microenvironment Cell Populations (MCP)-counter method [72]. This MCP-counter approach deconvoluted the RNA-seq data into absolute abundance scores for 8 major immune cell types (CD3+ T cells, CD8+ T cells, cytotoxic lymphocytes, NK cells, B lymphocytes, monocytic lineage cells, myeloid dendritic cells, and neutrophils) and two non-immune cell types (endothelial cells and fibroblasts) [64, 72]. These deconvoluted profiles subsequently underwent hierarchal clustering on unsupervised analysis [64]. Relative gene expression intensity was based on deviation from the mean per gene and was denoted by z scores (e.g. z score of 2 signifies gene expression of 2 standard deviations above the mean while a z score of -2 signifies gene expression of 2 standard deviations below the mean) on the generated transcriptomic heatmaps. Similarly, abundance scores were graded based on z scores.

Multiplex immunofluorescence

When tissue was available, multiplex immunofluorescent (mIF) panel staining and image analysis was performed at the Translational Molecular Pathology Immunoprofiling Lab at MD Anderson Cancer Center on one unstained 5 μ m section. The PD-L1/PD-1/TIL panel for carcinomas was performed on the 5 μ m sections as previously described [73-76].

Table 2 - Multiplex immunofluorescent panel

PD-L1/PD-1 and TIL panel

PD-L1
CD68
PD-1
CD8
CD3
AE1/AE3
DAPI

The Opal 7 multiplex kit (Perkin Elmer, Waltham, MA) was utilized in accordance with the manufacturer's protocol as previously described [73].

- 1) Deparaffinization of the section was performed
- 2) The section were placed in a container antigen retrieval buffer and microwave technology (EZ-Retriever ® system microwave; Bio-Genex, San Ramon, CA) was utilized to bring the liquid to boiling at 100 C for 1 minute followed by microwaved at 75 C for an additional 75 C [73].
- 3) The sections were cooled for 15 minutes at room temperature then rinsed with deionized water and Tris-buffered saline with Tween 20 (TBST; Santa Cruz Biotechnology, Dallas, TX) followed by Tris-HCL buffer containing 0.1% Tween (Dako, catalogue #S3022) for 10 minutes at room temperature
- 4) Based on the mIF panel, sections were incubated with one of the following primary antibodies against PD-L1, CD4, CD8, CD3, PD-1, CD68, and AE1/AE3.

- 5) Sections were washed and incubated for 10 minutes at room temperature with anti-mouse or anti-rabbit secondary antibodies (Novocastra, Leica Biosystems) after successive washes in TBST
- 6) Sections were subsequently incubated at room temperature for 10 min with Alexa Fluor tyramides (PerkinElmer, Waltham, MA) included in the Opal 7 kit to detect antibody staining as per manufacturer's protocol
- 7) Steps 4 – 6 were completed to consecutively add antibodies for the respective mIF panels. For the PD-L1/PD-1/TIL panel, the sequence of antibody staining was AE1/AE3, PD-L1, PD-1, CD4, CD8, CD3, and CD8.
- 8) Following completion of the consecutive staining for the respective mIF panels, three additional washes were performed deionized water and the sections were counterstained with DAPI for 5 min and mounted with VECTASHIELD Hard Set (Vector Labs, Burlingame, CA).

Following completion of mIF panel staining, imaging analysis was performed using Vectra 3.0 spectral imaging system (PerkinElmer, Waltham, MA) as previously described [73-77]. MIF panel staining imaged by using the fluorescence protocol at 10 nm λ from 420 nm to 720 nm, to extract fluorescent intensity information from the images and scanned with the Vectra 3.0 spectral imaging system (PerkinElmer, Waltham, MA) [73]. The analysis was performed by a pathologist in the Translational Molecular Pathology Immunoprofiling Lab in five intratumoral areas using 660 μm x 500 μm (0.33mm²) region of interest at x20 magnification to cover a total intra-tumoral area of 1.65mm². Histologic evaluation of each region of interests was performed to ensure adequate tumor tissue was included (e.g. at least 85% malignant cells, AE1/AE3 positivity, and tumor stroma) [73]. When the 5 regions of interests did not cover

1.65mm² of intra-tumoral area, analysis was performed in greater than 5 regions in order to cover at least 1.65mm² if there are more intratumoral area available. Using the pancytokeratin (AE1/AE3) marker, the intratumoral area is compartmentalized into epithelial (tumor) and stromal compartments.

InForm ® image software (Akoya Biosciences, Malborough, MA) was utilized following section image capture and each individual unmixed staining was combined by using the spectral library information to associate each fluorochrome component with a mIF component [73]. InForm image analysis software enabled characterization and quantification (expressed in average of cell densities from analyzed areas in mm² (n/mm²)) of immune cell subpopulations per panel [73].

Statistical analysis

Demographic and clinicopathologic characteristics of the study population were summarized with standard descriptive statistics. Chi-squared and Fischer's exact test were performed where applicable. A p-value of less than 0.05 was defined as statistically significant. Box plots were utilized to compare differences among samples in regards to mRNA expression levels and cell counts/abundance scores. The statistical significance of the differences were evaluated using non-parametric Mann-Whitney U test and Fischer's exact test where applicable. The Spearman's rank correlation coefficient was used to calculate the association between two continuous variables. The Benjamini-Hochberg method was used to adjust for false discovery rate (FDR) and an adjusted FDR p-value <0.05 was considered statistically significant [78]. Response to pembrolizumab was evaluated through best radiologic response to treatment (responders were patients who had partial or complete response to treatment while non-responders had transient stable disease (<6 months) or disease

progression). PFS was defined from start of treatment until date of disease progression or death. Those alive and without disease progression were censored at their date of last follow-up. OS was defined from start of treatment until date of death. Those alive were censored at their date of last follow-up. The product limit estimator of Kaplan-Meier was used to estimate PFS and OS. Kaplan-Meier estimates. Clinical descriptive and survival analyses were performed using Stata/MP v16.0 (StataCorp, College Station, TX). Bioinformatics analyses were performed were performed utilizing R statistical package (RStudio, Boston, MA).

Results

Clinicopathologic characteristics

Tumor specimens analyzed were from 11 patients in the untreated cohort and 23 patients in the treated cohort. In the untreated cohort, samples were obtained from the gynecologic oncology tumor bank and consisted on 11 fresh-frozen tumor samples. The characteristics of the patient population are shown in **Table 3**. The median age was 66 years old and most tumors were grade 2 and all tumors were endometrioid histology (100%). The majority of patients had early stage disease (63.6%) and had MLH1 promoter methylation as the MSI-H cause.

Table 3 - Clinicopathologic characteristics of the untreated cohort

	N (%)
Age (years)*	66 (54 – 66)
BMI (kg/m ²)*	31.6 (21.1 – 35.6)
Tumor grade	
2	9 (81.8%)
3	2 (18.2%)
Histology	
Endometrioid	11 (100%)
Stage	
1	7 (63.6%)
2	1 (9.1%)
3	2 (18.2%)

4	1 (9.1%)
Cause of MSI-H	
MLH1 promoter methylation	10 (90.9%)
Somatic loss of MMR protein	1 (9.1%)

Table 3 legend: BMI = body mass index. MMR = mismatch repair. MSI-H = microsatellite instability high. *Represented in median (range).

In the 23 patients of the treated cohort, there were 33 FFPE samples (21 primary and 12 recurrent specimens) obtained for the study. The characteristics of the patient population are demonstrated in **Table 4**.

Table 4 - Clinicopathologic characteristics of the treated cohort

		Evaluable patients (n=21)	
	Overall (n = 23)	Responders (n = 14)	Non-responders (n = 7)
Age (years)*	59 (40 – 77)	61 (40 – 77)	57 (45 – 67)
BMI (kg/m ²)*	31.1 (18.6 – 51.8)	32.3 (23.3 – 47.3)	27.1 (18.6 – 51.8)
Tumor grade			
2	13 (59.1%)	6 (42.9%)	5 (71.4%)
3	9 (40.9%)	8 (57.1%)	1 (14.3%)
Histology			
Endometrioid	18 (78.3%)	11 (78.6%)	5 (71.4%)

Mixed	4 (17.4%)	3 (21.4%)	1 (14.3%)
Adenocarcinoma NOS	1 (4.4%)	0 (0.0%)	1 (14.3%)
Initial stage			
1	9 (40.9%)	4 (28.6%)	4 (57.1%)
2	1 (4.6%)	1 (7.1%)	0 (0.0%)
3	7 (31.8%)	6 (42.9%)	1 (14.3%)
4	5 (22.7%)	3 (21.4%)	2 (28.6%)
Cause of MSI-H			
MLH1 promoter methylation	15 (65.2%)	11 (78.6%)	4 (57.1%)
Loss of MMR protein	5 (21.7%)	2 (14.3%)	3 (42.9%)
MSI marker positive	1 (4.4%)	0 (0.0%)	0 (0.0%)
Germline MMR defect	2 (8.7%)	1 (7.1%)	0 (0.0%)
Prior lines of systemic therapy*	1 (1 – 4)	1 (1 – 4)	2 (1 – 4)
Treatment cycles of pembrolizumab*	9 (2 – 35)	12 (2 – 35)	5 (2 – 6)
Vitality status			
Alive	19	14	3
Deceased	4	0	4

Table 4 legend: BMI = body mass index. MMR = mismatch repair, MSI-H microsatellite instability high. NOS = not otherwise specified. *Represented in median (range).

Overall, the median age was 59 years old and the majority of patients had endometrioid histology (78.3%). MLH1 promoter methylation was the common cause of MSI-H. The median number of prior lines of systemic therapy was 1 and the median number of cycles of pembrolizumab was 9. Among the 23 patients who were treated with pembrolizumab, there were 14 responders, 7 non-responders, and 2 patients without evaluable response to pembrolizumab. There were no significant differences between responders and non-responders for age ($p = 0.157$), BMI ($p = 0.307$), tumor grade ($p = 0.157$), histology subtype ($p = 0.499$), initial stage ($p = 0.515$), cause of MSI-H ($p = 0.397$), and prior lines of systemic therapy ($p = 0.122$).

Among the 21 patients with evaluable response to pembrolizumab, there were 7 disease progressions and 6 deaths. The overall median follow-up was 18.5 months (range 2.5 – 46.1). The median PFS was Kaplan-Meier curves for PFS and OS are demonstrated based on response to treatment in **Figure 3** and **Figure 4**, respectively. The median PFS and OS for the non-responders were 3.3 and 20.6 months, respectively. The median PFS, OS, and duration of response for the responders were not reached.

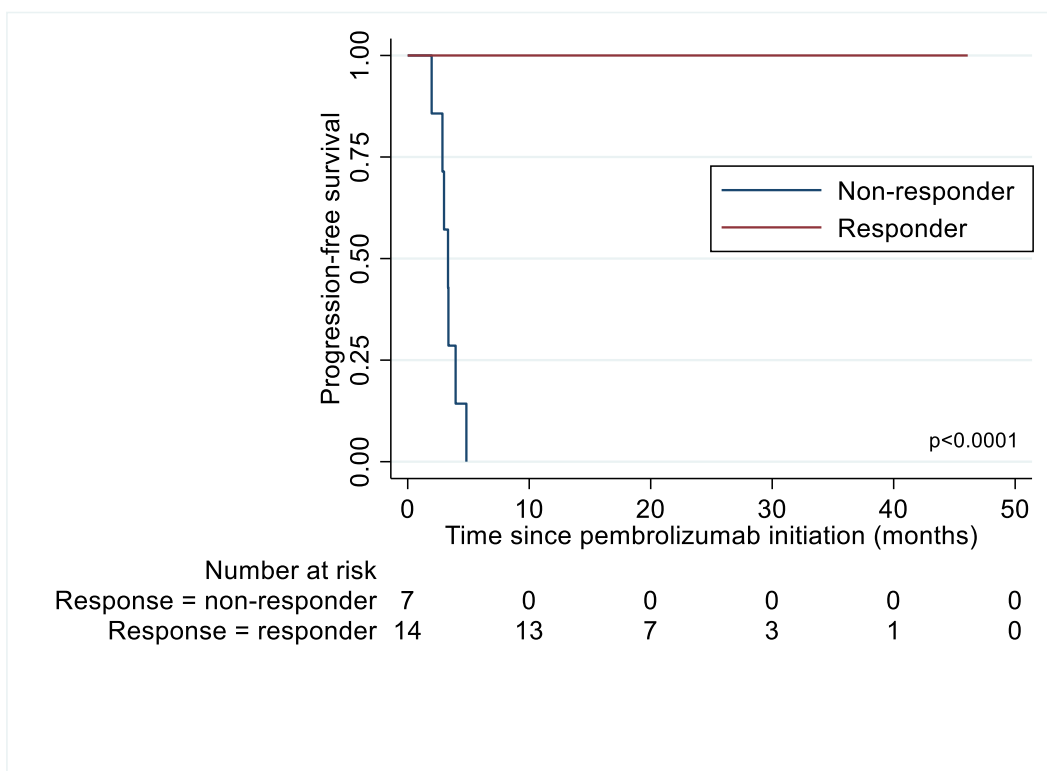


Figure 3 - Progression-free survival by response to pembrolizumab

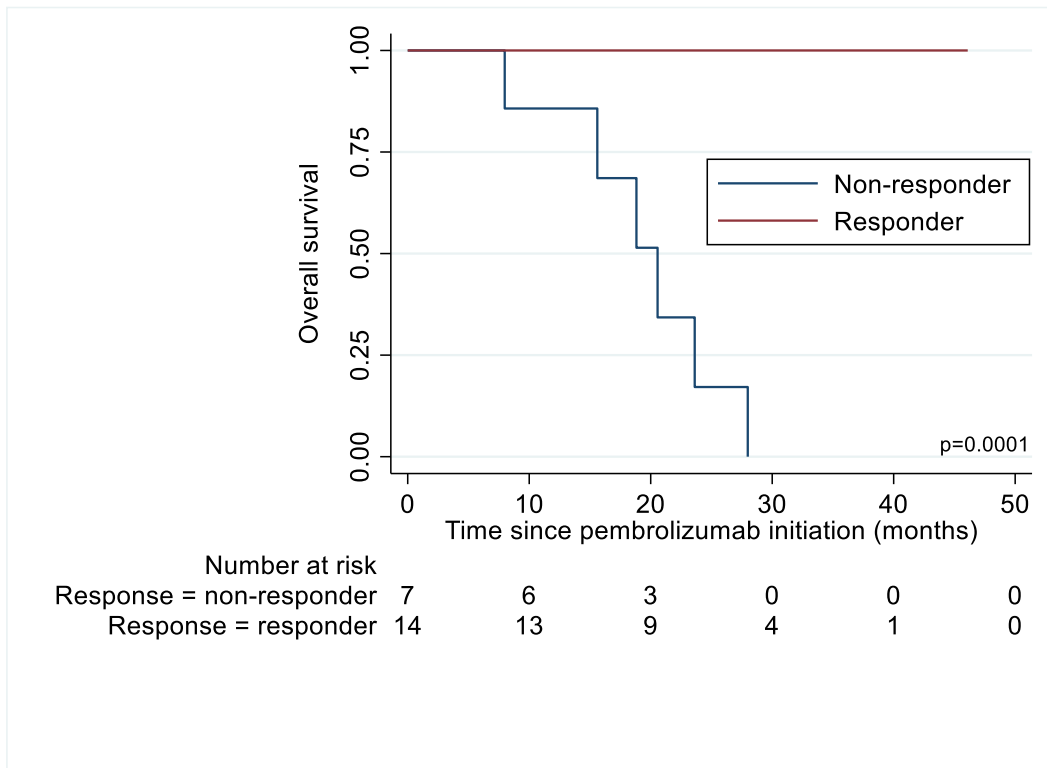


Figure 4 - Overall survival by response to pembrolizumab

MSI-H endometrial TMEs display a diversity of immune cell subpopulations

Figure 5 demonstrates the heatmap for 11 tumor samples from the untreated cohort where RNA-seq was performed. The heatmap demonstrates segregation of TME into three subtypes based on transcriptomic profiles. In the “hot” subtype (n = 4), tumors with this classification had strong signals for T cells (including cytotoxic T-cells), B cells, NK cells, monocytes, neutrophils, and dendritic cells. For the “cold” subtype (n = 3), these tumors had low signals for the aforementioned immune cell populations. In the “warm” subtype (n = 4), the tumors had transcriptomic profiles showing moderate signals for these anti-tumor cells. However, there was an enrichment for fibroblasts and endothelial cells in the “warm” TME subtype.

Transcriptomic signatures in the TME shape response to pembrolizumab

Figure 6 demonstrates the transcriptomic profile of tumors in the treated cohort that underwent EC-RNA-seq. Based on gene expression, the tumors could be generally segregated into 3 general categories as seen in the untreated cohort: “hot” (n = 7), “cold” (n = 16), and “warm” (n=10). Tumors within the “cold” subtype could be further subdivided into the subcategories with an enrichment (“cold1”; n =11) or paucity (“cold2”; n=5) of endothelial cells and fibroblasts. There were 21 patients who had evaluable responses to pembrolizumab. All tumors in the “hot” or “cold2” had a response to pembrolizumab (**Figure 6**).

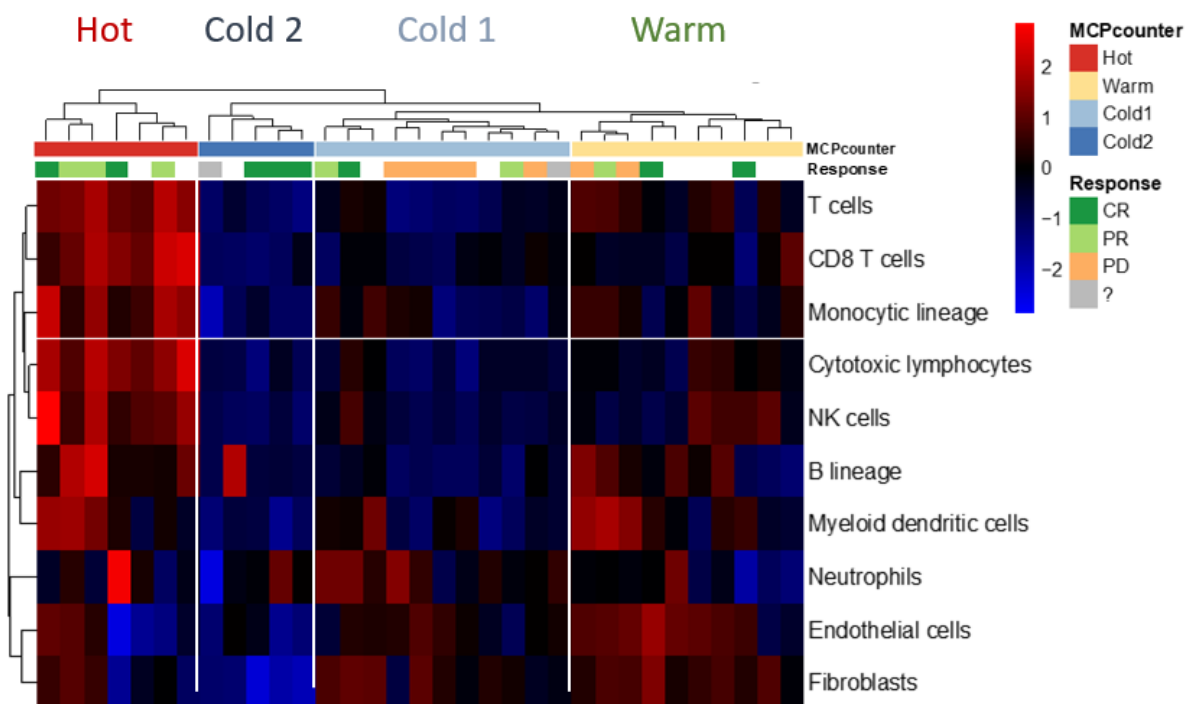


Figure 6 - Transcriptomic profile of MSI-H endometrial tumors in the treated cohort. TMEs could be subdivided into 3 general subtypes based on intensity of anti-tumor immune cell activity: “hot”, “warm”, or “cold” subtypes. “Cold” subtypes could be further sub-classified based on an enrichment (“cold1”) or paucity (“cold2”) of

fibroblasts and endothelial cells. CR = complete response. PD = disease progression. PR = partial response. ? = unknown response.

There were 3 partial and 2 complete responses in the evaluable “hot” tumors; there were no non-responders were observed in this TME subtype. In the “cold” and “warm” subtypes, there were 3 partial (2 “warm” and 1 “cold1” and 6 complete (1 “warm,” 2 “cold1,” and 3 “cold2”) responders. In these groups, there were 7 non-responders (5 “warm” and 2 “cold1”).

Endothelial cells and fibroblasts in the TME are associated with poor response to pembrolizumab

Endothelial cell and fibroblasts appeared to be enriched in the TME of the “cold1” and “warm” subtypes. Evaluating response based on enrichment of endothelial cells and fibroblasts, patients were subdivided into a fibroblastic (n = 13) or non-fibroblastic group (n = 8) (**Figure 7**). Non-responders are more likely to have an enrichment of fibroblasts and endothelial cells in the TME (p = 0.018).

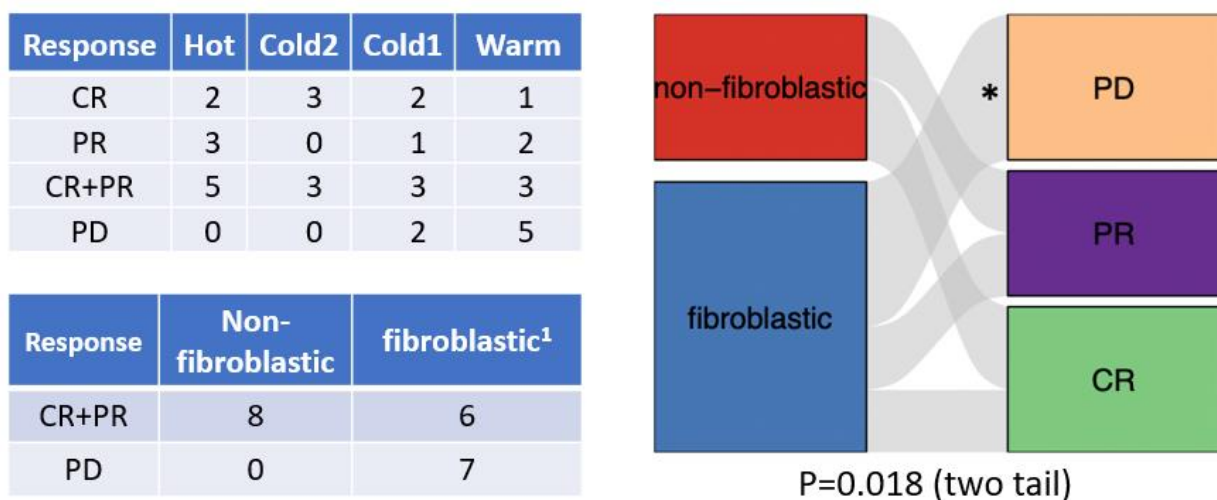


Figure 7 - Response to pembrolizumab based on tumor microenvironment.

¹Fibroblastic = enrichment of endothelial cells and fibroblasts in the TME. CR = complete response. PD = progression of disease. PR = partial response. TME = tumor microenvironment.

Figure 8 and **Figure 9** demonstrate endothelial cell and fibroblast marker gene expression for responders vs. non-responders and complete responders vs. partial responders vs. non-responders, respectively. There was a significant increase in gene expression of two endothelial cell (HHIP and MMRN1) and fibroblast (PAMR1) genes

(Figure 8). Endothelial cell (TEK, MYCT1, EMCN, PTPRB, KDR, and PEAR1) and fibroblast (TAGLN) expression was inversely correlated with response **(Figure 9).**



Figure 8 - Endothelial cell and fibroblast marker gene expression (responders vs non-responders). **Red boxes indicate statistical significance.** CR = complete response. PD = disease progression. PR = partial response.



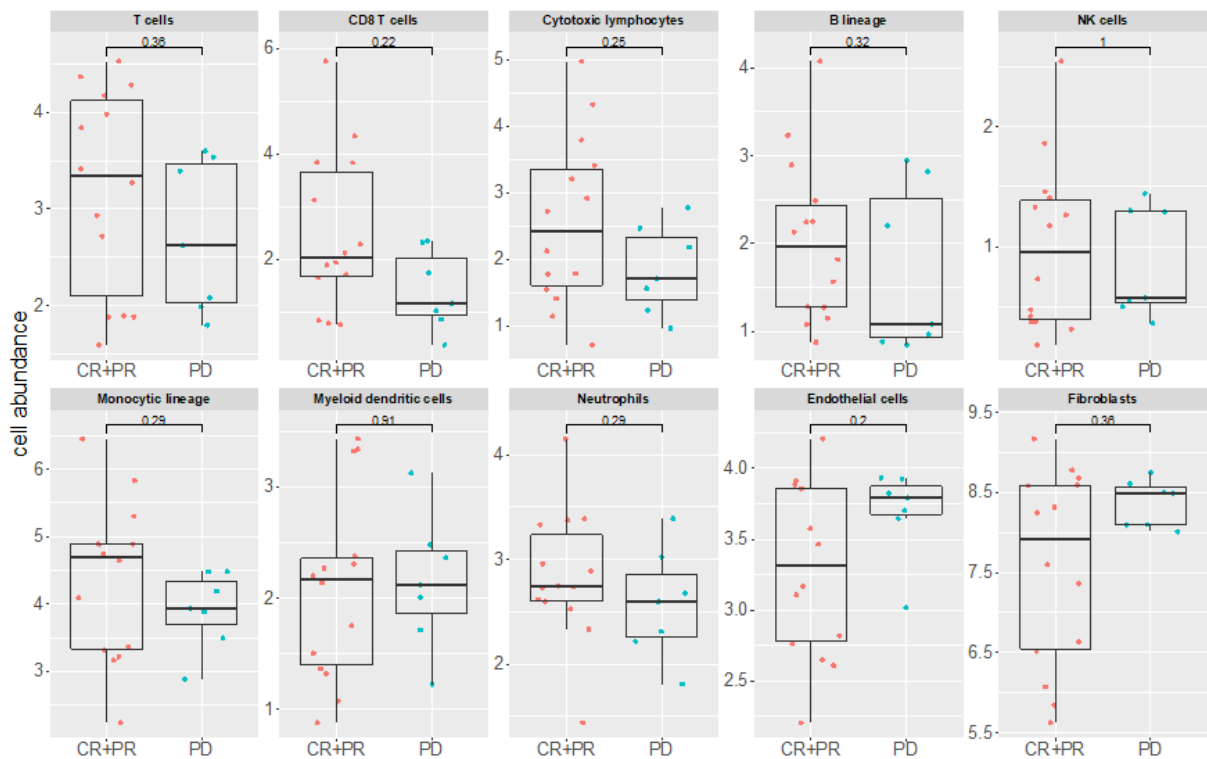
Figure 9 - Endothelial cell and fibroblast marker gene expression by response

type. Red boxes indicate trend of rising gene expression with decreasing response to

pembrolizumab. CR = complete response. PD = disease progression. PR = partial response.

Additionally, response to pembrolizumab was inversely correlated with endothelial cell and fibroblast abundance with complete responders having the least amount of endothelial cells and fibroblasts (**Figure 10**). For T cells, B cells, NK cells, myeloid dendritic cells, neutrophils, and cells of monocytic lineage, there were no trends observed with response to treatment.

A)



B)

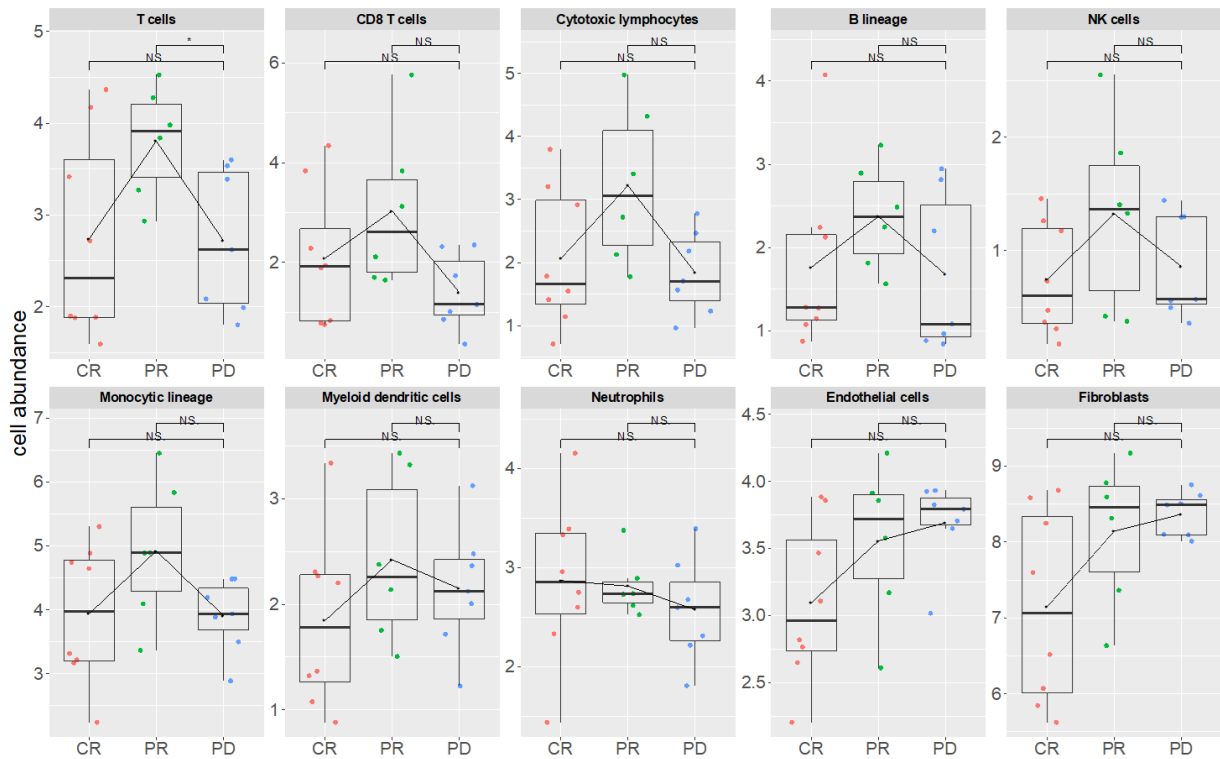


Figure 10 - Immune cell subpopulation and response to pembrolizumab. A)

Responders vs non-responders. B) Complete responders vs partial responders vs non-responders. CR = complete response. PD = disease progression. PR = partial response.

Differential gene expression tumors with endothelial cell and fibroblast enrichment in the TME

Figure 11 is a volcano plot that describes differential gene expression between the tumors with enrichment (fibroblastic) or paucity (non-fibroblastic) of endothelial cells and fibroblasts in the TME. In the non-fibroblastic group, there were 117 genes that were differentially highly expressed. These included immune system associated genes

involving in IFN- γ signaling and its downstream response and regulatory elements, NK cell mediated cytotoxicity, cytokine signaling, and response elements to IFN- α signaling, Other highly expressed genes included those involved in solute carrier transporter disorders, SUMOylation of ubiquitylation proteins, disorders of transmembrane transporters, and nuclear envelope breakdown. In the fibroblastic group, there were 230 genes that were differentially highly expressed. These genes included those involved in myogenesis and muscle contraction (skeletal, vascular, and smooth muscle). Other highly expressed genes included those involving cellular adhesions/interactions (cell-extracellular matrix interactions, cell junction organization, cell-cell communication, focal adhesion, and apical junction complex) and other genes involved in epithelial mesenchymal transition, wound healing, fibrosis, and metastasis.

TME is a prognostic biomarker for survival following pembrolizumab therapy

Among the 21 patients with evaluable response to pembrolizumab, there were 7 disease progressions and 6 deaths. The overall median follow-up was 18.5 months (2.5 – 46.1). The Kaplan-Meier curves for PFS and OS (based on TME and fibroblastic group status) are shown in **Figure 12** and **Figure 13**, respectively. Approaching statistical significance, tumors that had “hot” or “cold2” TMEs had the highest PFS followed by “cold1” and “warm” TMEs ($p = 0.051$). For OS, there was no difference between TMEs ($p = 0.272$). Based on fibroblastic status, the fibroblastic group had significantly worse PFS ($p = 0.016$) compared to the non-fibroblastic group. There was also a trend towards worse OS in the fibroblastic group ($p = 0.057$).

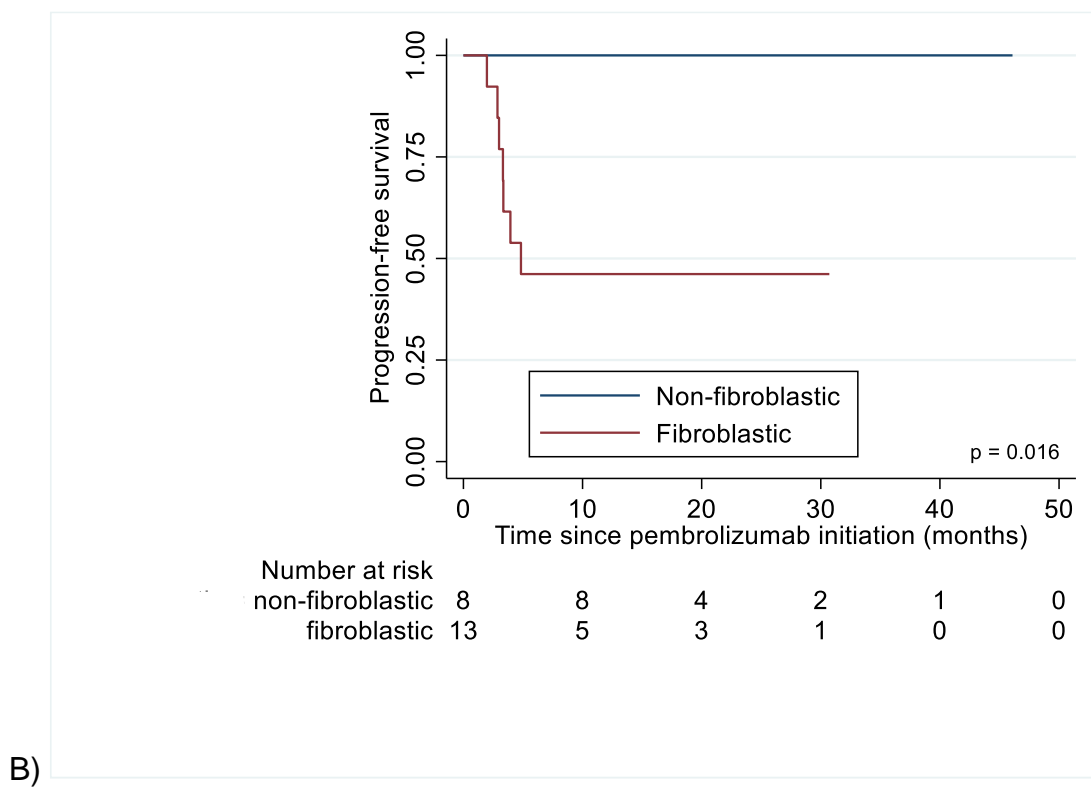
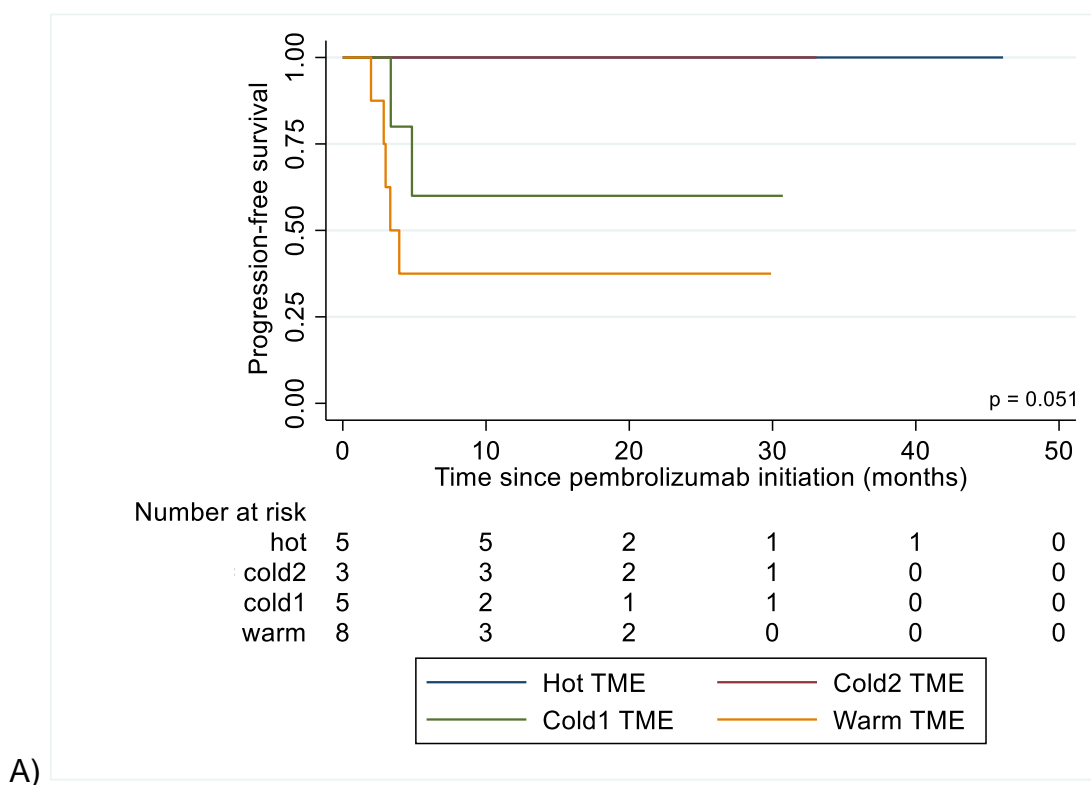
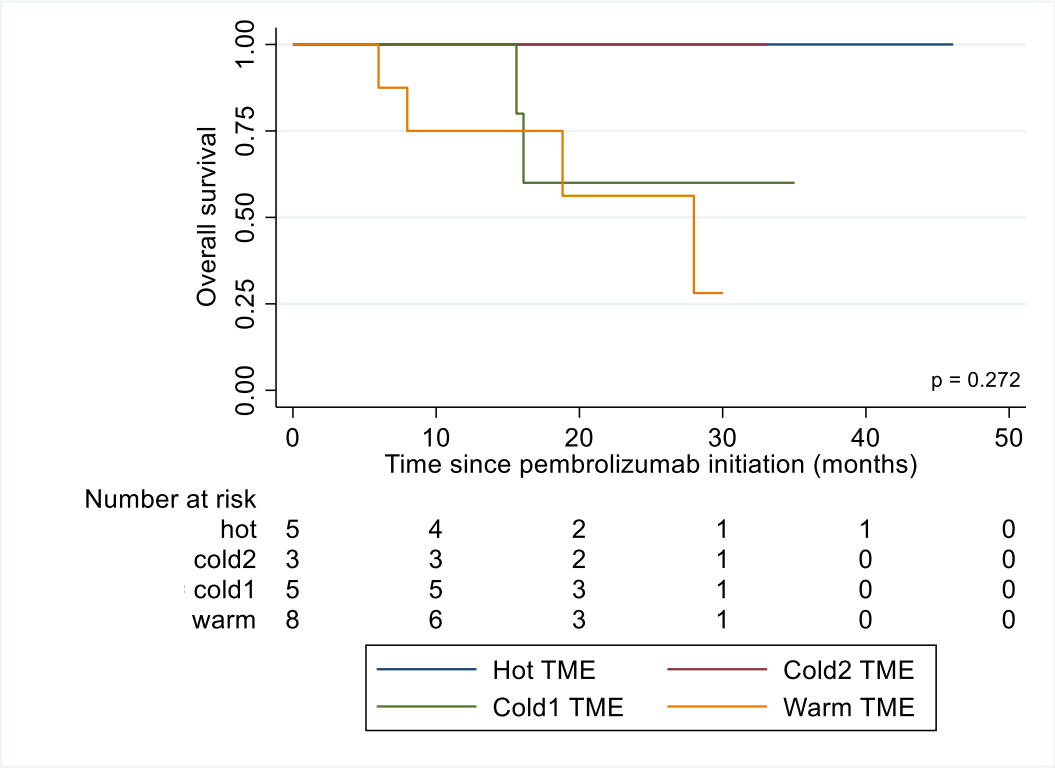
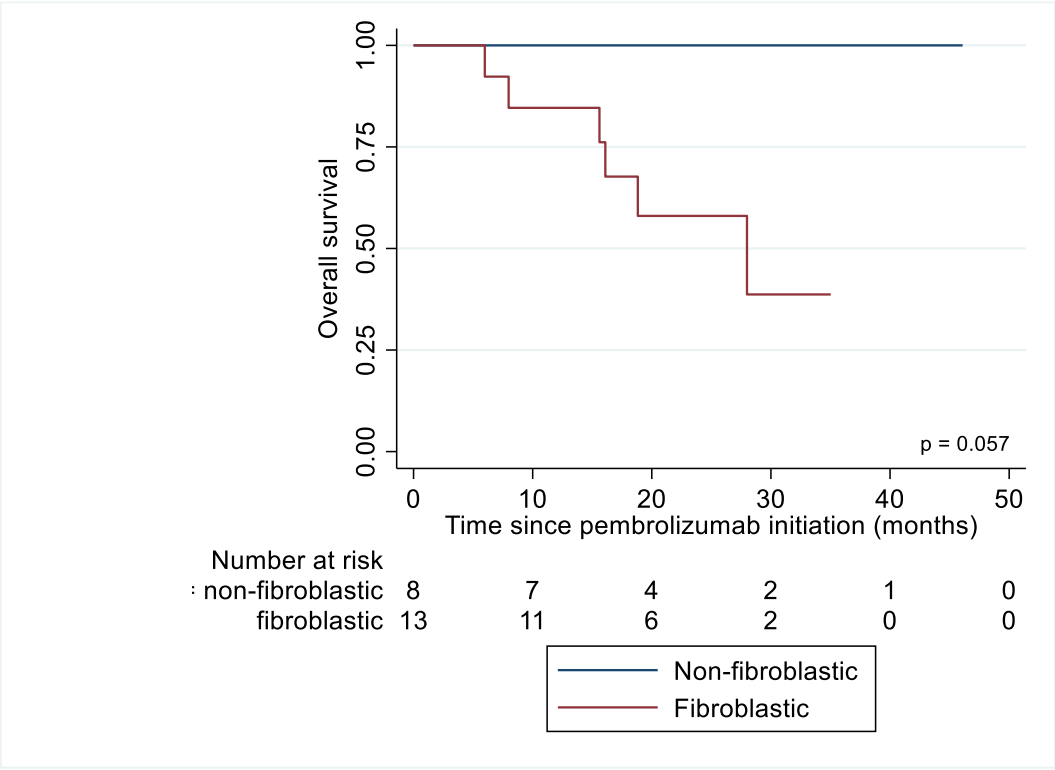


Figure 12 - Progression-free survival based on tumor microenvironment subtype and fibroblastic group status. A) PFS based on TME subtype B) PFS based on fibroblastic group status



A)

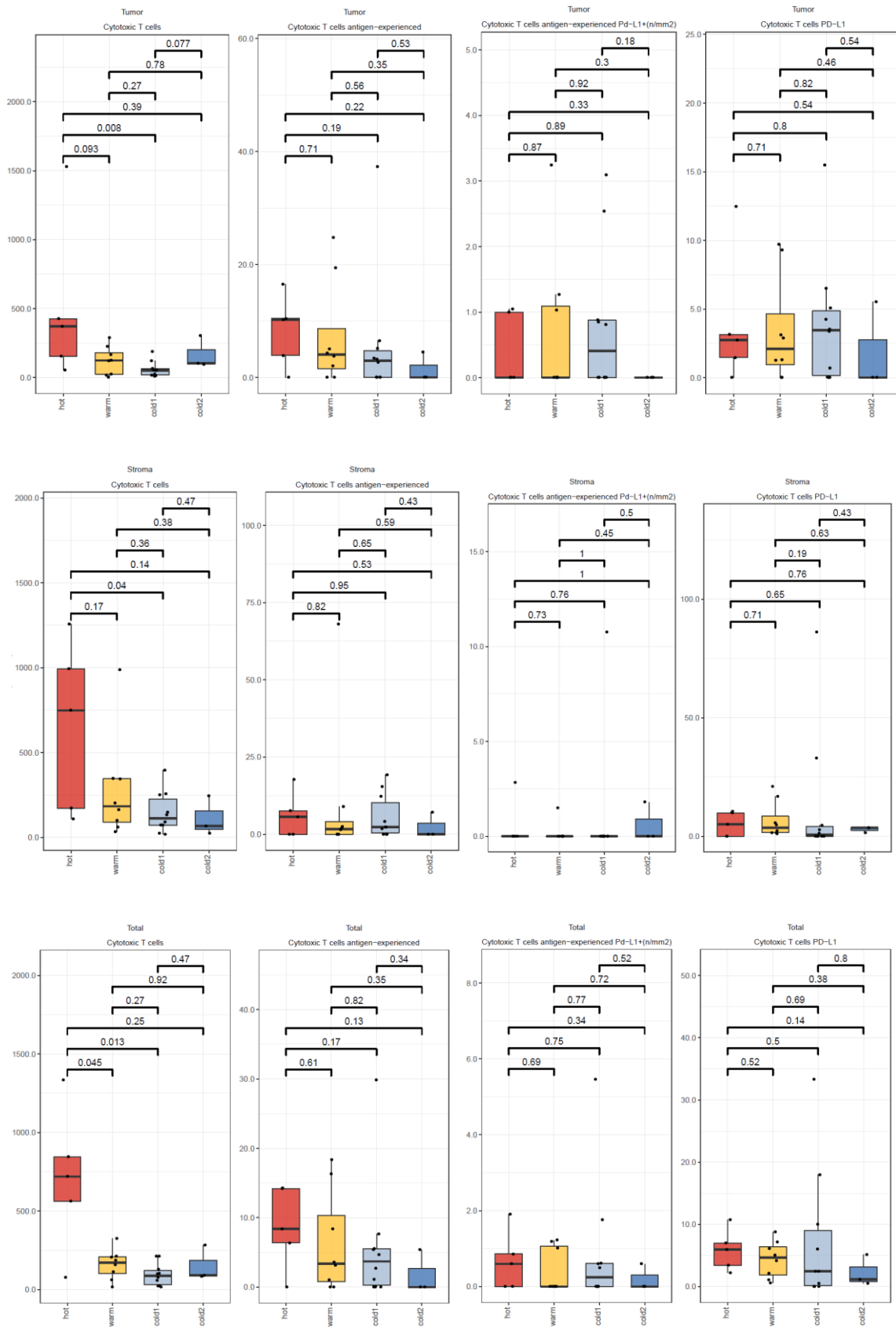


B)

Figure 13 - Overall survival based on tumor microenvironment subtype and fibroblastic group status. A) OS based on TME subtype B) OS based on fibroblastic group status

PD-L1/PD-1/TIL mIF testing

There were 27 samples (19 primary and 8 recurrent) from 21 patients that were evaluated using PD-L1/PD-1/TIL mIF panel testing. Staining was successful in all but in one sample which had only necrotic tissue without malignant cells; this sample belong to a patient without evaluable response to pembrolizumab. Evaluating cytotoxic T cells (CD3⁺ CD8⁺) in the combined tumor and stromal compartments, the “hot” TME samples had the highest cell density compared to the “warm” ($p = 0.045$) and “cold1” ($p = 0.013$) TME samples (**Figure 14**). T lymphocytes (CD3⁺ cells) cell density appeared to be greater in “hot” TME samples and reached statistical significance when compared to “cold1” TME samples ($p = 0.008$) (**Figure 14**). Antigen experienced T cells with (CD3⁺PD-1⁺PD-L1⁺) or without PD-L1 positivity (CD3⁺PD-1⁺) were similar across all TME subtypes (**Figure 14**). T lymphocytes and marker subcategories did not differ by response to pembrolizumab (**Figure 15**).



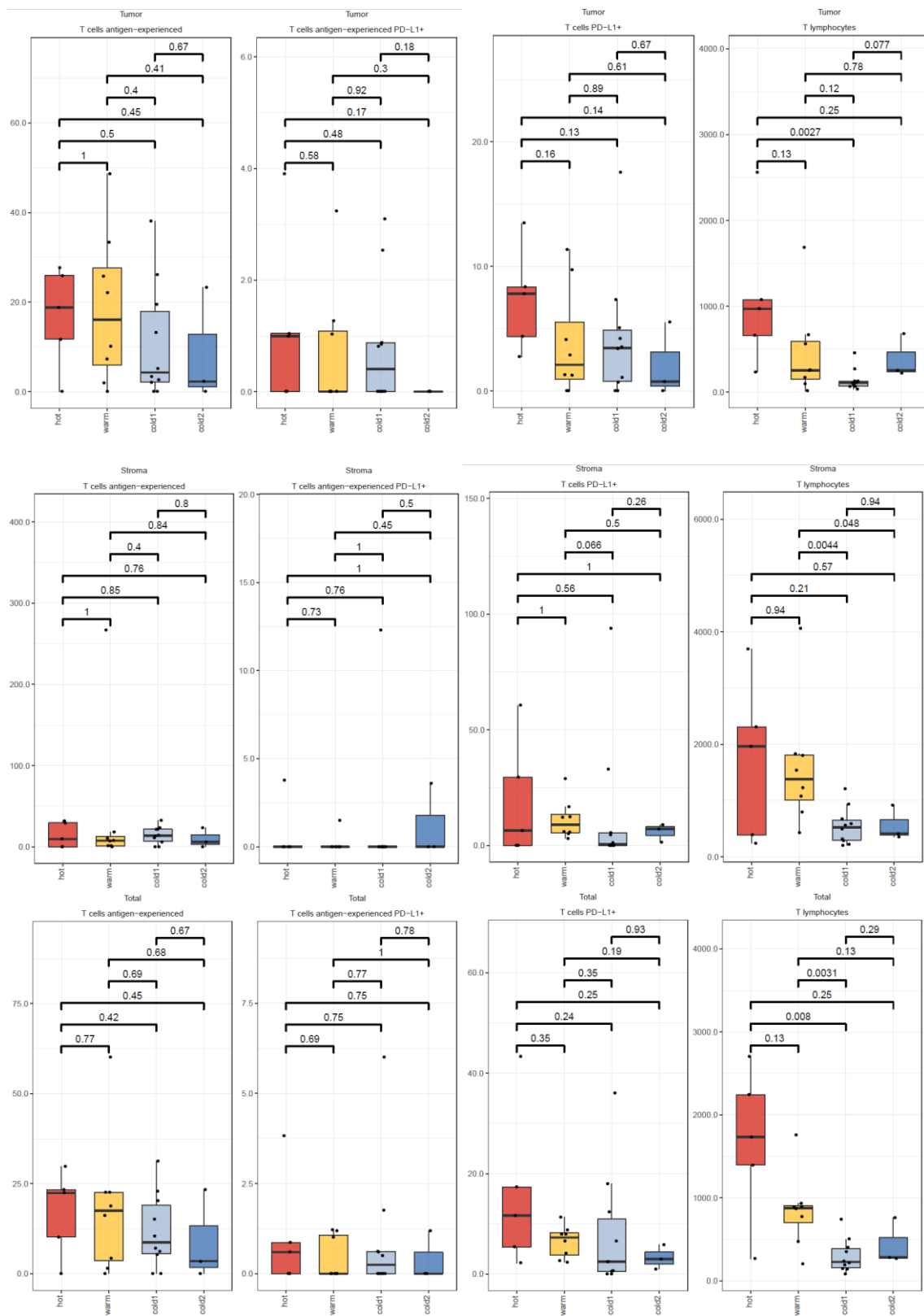
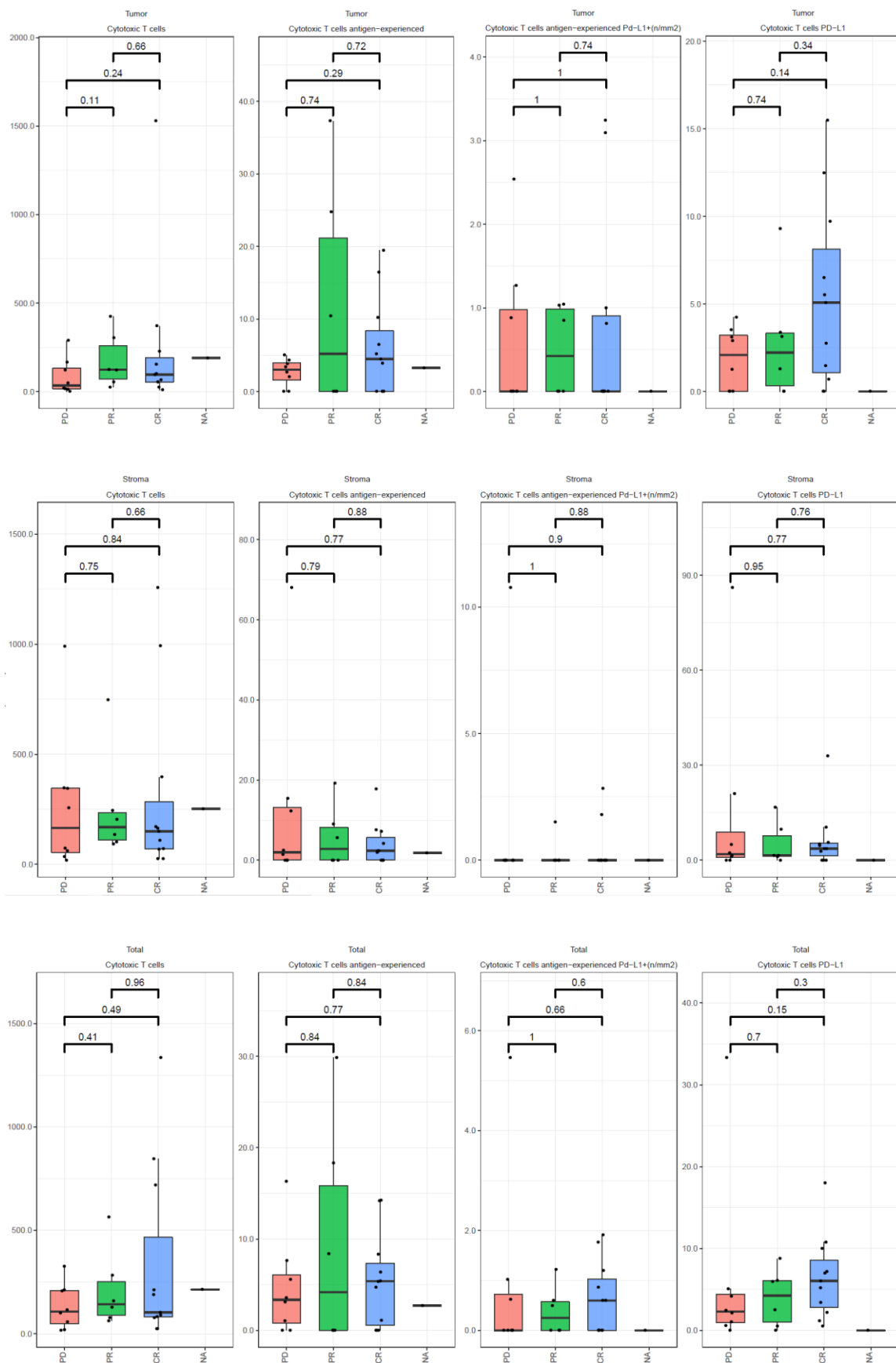


Figure 14 - T lymphocytes by tumor microenvironment subtype



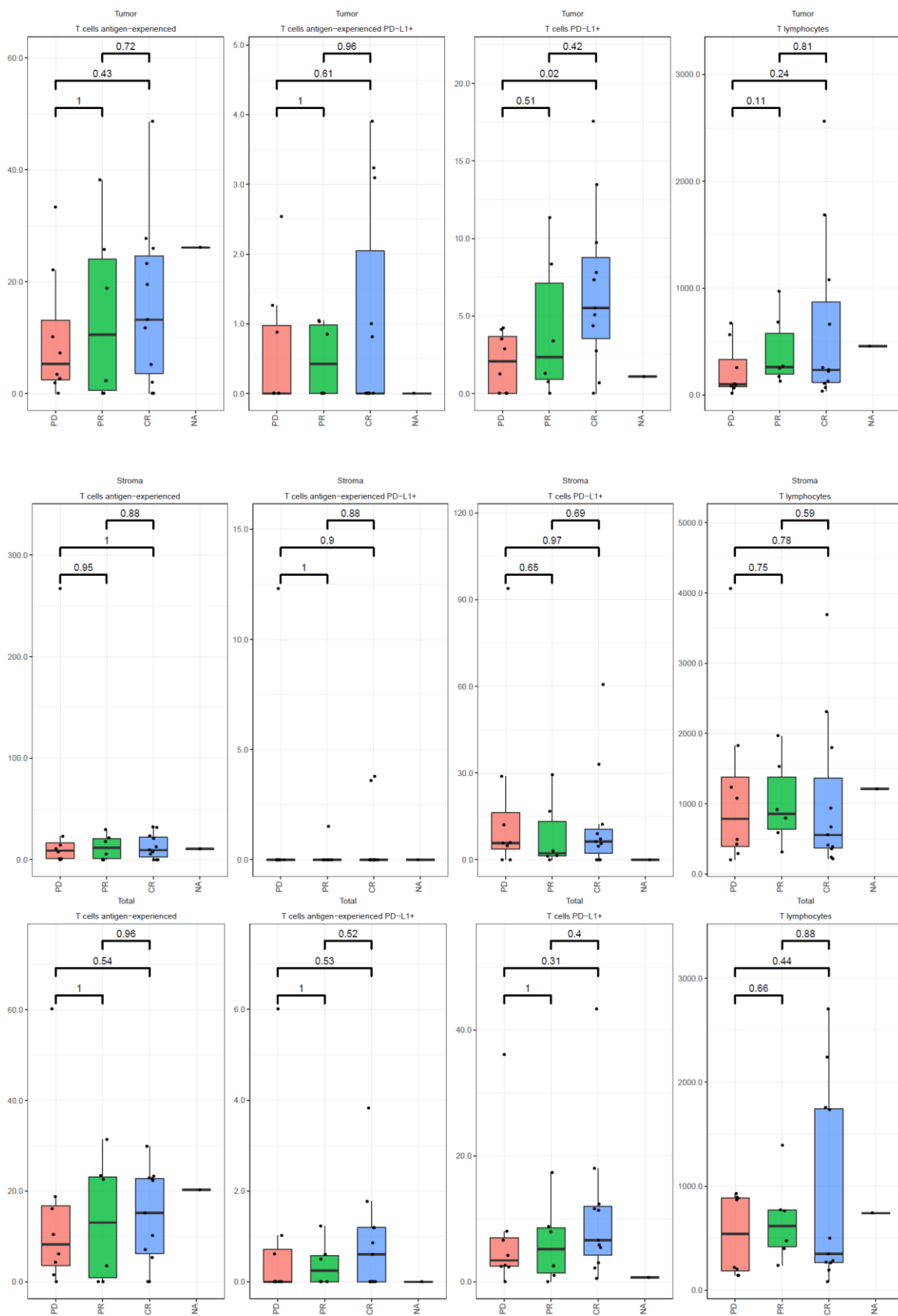
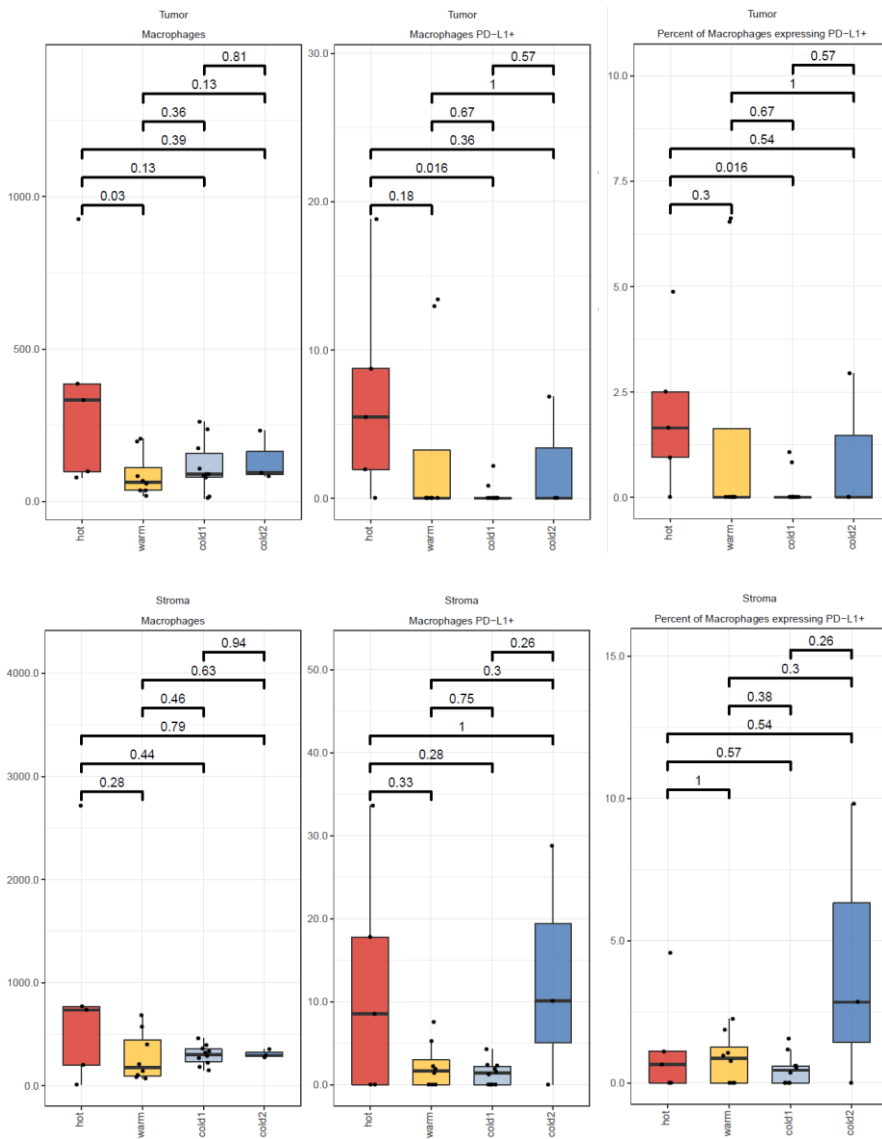


Figure 15 - T lymphocytes by response

Staining for macrophages (CD68⁺) with or without PD-L1 positivity are shown by TME (**Figure 16**) and response (**Figure 17**). Cell densities for total macrophages were higher in the “hot” TME subtype compared to the “warm” TME subtype ($p = 0.03$) (**Figure 16**). CD68⁺PD-L1⁺ macrophages were higher in the “hot” TME subtype compared to the “cold1” TME subtype ($p = 0.016$) (**Figure 16**). When evaluating the macrophage population by response, partial responders had significantly higher total macrophages ($p = 0.029$), PD-L1⁺ macrophages ($p = 0.012$), and percentage of macrophages expressing PD-L1⁺ ($p = 0.012$) compared to non-responders (**Figure 17**). Additionally, similar trends were observed with complete responders ($p = 0.07$). When evaluating PD-L1 positivity in malignant cells, there were no differences in TME subtypes or response to pembrolizumab (**Figure 18**).



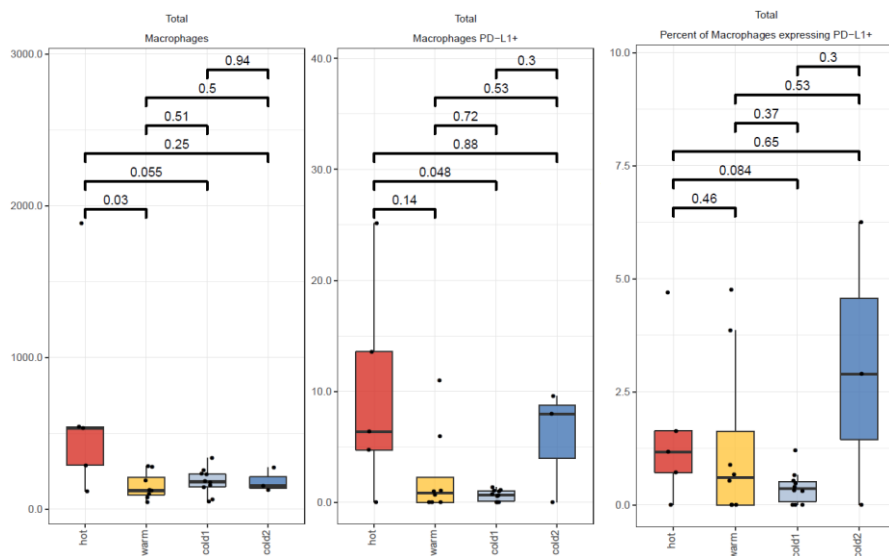


Figure 16 - Macrophages population by tumor microenvironment

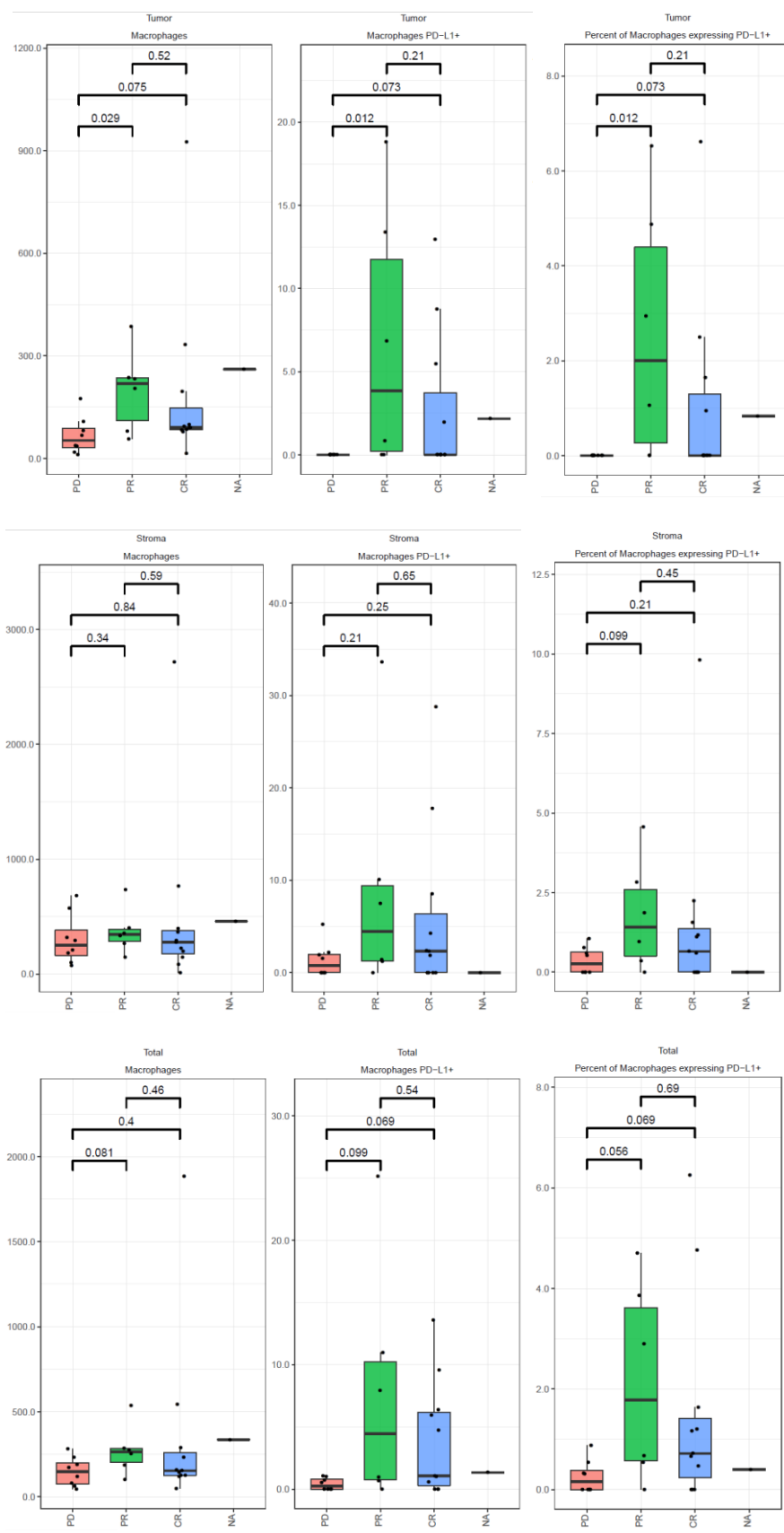


Figure 17 - Macrophage population by response

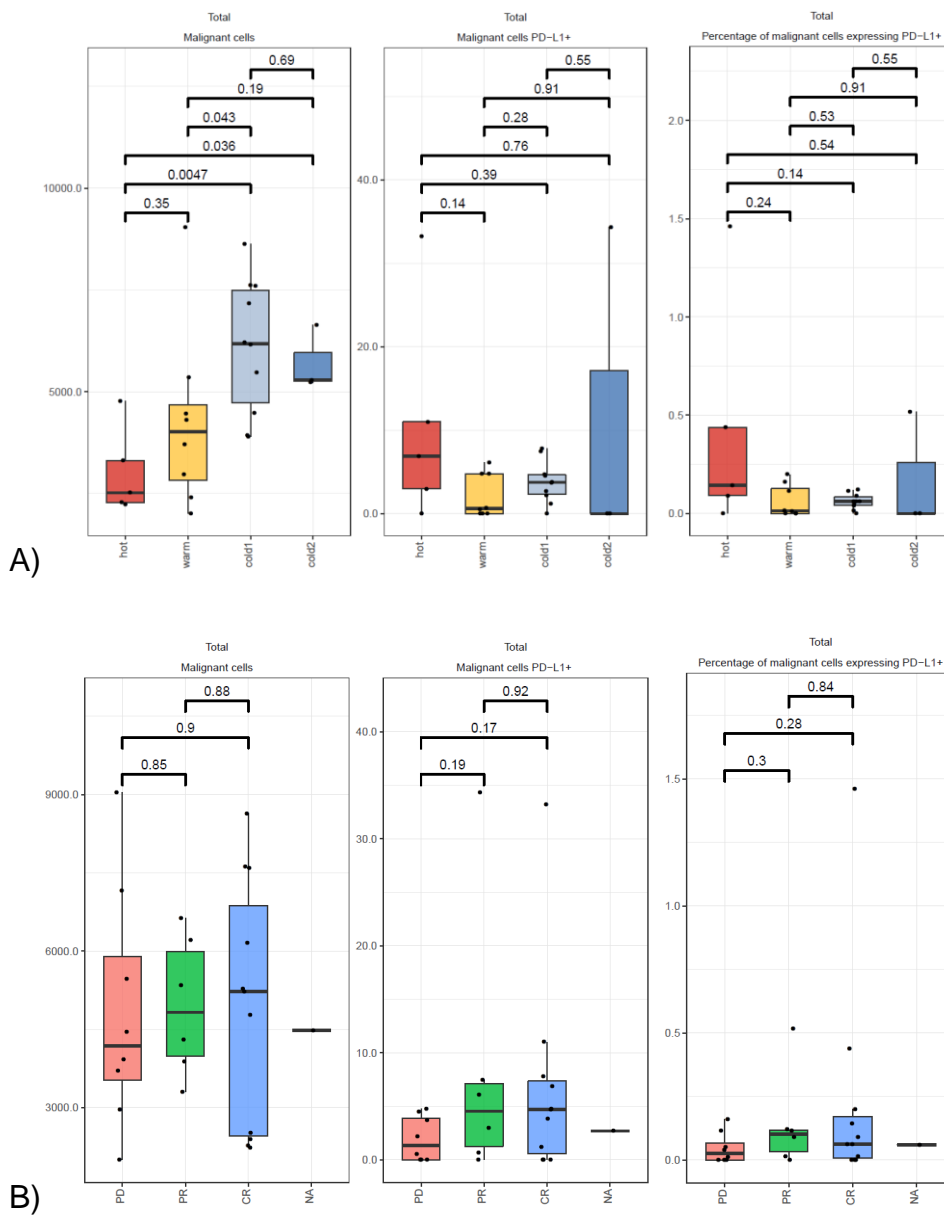


Figure 18 - PD-L1 positivity in tumor cells. A) PD-L1⁺ tumor cells by TME B) PD-L1⁺ tumor cells by response

Discussion

With the risk of potential life threatening treatment-related adverse events from pembrolizumab, it is essential to determine biomarkers that will select patients who will derive the greatest benefit from treatment [35]. This thesis sought to evaluate the TME of MSI-H endometrial tumors and explore potential biomarkers of response to pembrolizumab. In both the untreated and treated cohort datasets, the transcriptomic profiles demonstrated heterogeneity of TME across MSI-H endometrial tumors. Based on immuno-genomic signatures, TMEs could be subdivided into “hot,” “cold,” and “warm” subtypes. Additionally, “cold” subtypes could be further subclassified into two types based on enrichment (“cold1”) or paucity (“cold2”) of endothelial cells and fibroblasts in the TME. The majority of prior studies that have broadly profiled endometrial tumors but have not focused on teasing out immune-genomic differences and variations within MSI-H tumors [16, 79, 80]. However, in a study by Pakish and colleagues, the researchers compared the immune microenvironment of MSI-H endometrial tumors attributable to sporadic vs. inherited Lynch syndrome origin [81]. Utilizing mIF panels on archival tumor samples, the researchers demonstrated TME heterogeneity where sporadic MSI-H endometrial tumors had higher total macrophages (with or without PD-L1⁺ expression) in the stroma and tumor compared to Lynch syndrome associated MSI-H endometrial tumors[81]. Additionally, sporadic MSI-H endometrial tumors had fewer cytotoxic T cells in the stroma compared to Lynch syndrome associated MSI-H endometrial tumors [81]. Despite demonstrating differing TMEs among sporadic and Lynch Syndrome associated MSI-H endometrial tumors, it remains to be determined how it shapes PD-1 inhibitor response [81].

Additionally, this thesis evaluated transcriptomic profiles in pre-treatment endometrial tumor samples (treated cohort) to correlate TME with response to subsequent pembrolizumab therapy. Therapeutic benefit to pembrolizumab was observed in the responders to treatment in this cohort where all 14 patients who responded had no disease progression (either were cured or had stable disease) on radiologic assessment. Furthermore, the characteristic of the TME also shaped response and prognosis for patients treated with pembrolizumab. As anticipated, all 5 patients with “hot” TME subtypes achieved response to pembrolizumab therapy. MIF panel testing mirrored the RNA-seq analysis and demonstrated higher T lymphocytes, cytotoxic T cells, and leukocytes in hot subtype compared to the other TME subtypes. Interestingly, total macrophages and PD-L1⁺ macrophages were significantly associated with responders compared to non-responders. Prior studies have reported poorer survival outcomes in endometrial cancer when associated with higher CD68⁺ macrophage cell densities in the TME but these have not been in the context of immunotherapy treatment [82-84]. Although published in non-small cell lung cancer, one recent publication has demonstrated that increased correlation of PD-L1⁺ macrophages and level of infiltration with cytotoxic T cells and improved response to PD-1 inhibitors [85].

Among the 4 TME subtypes previously described, the TMEs could be grouped into fibroblastic or non-fibroblastic groups based on the enrichment of fibroblasts and endothelial cells in the TME. Patients with fibroblastic TMEs were more likely to have treatment refractory responses to pembrolizumab compared to those with non-fibroblastic TMEs ($p = 0.018$). Furthermore as therapeutic response to pembrolizumab declined, there was a trend of increasing fibroblast and endothelial cell enrichment.

Additionally, supervised analysis of fibroblastic vs. non-fibroblastic tumors demonstrated that there was significantly higher expression of genes regulating cellular adhesions/interactions and myocytes coupled with reduced expression of IFN- γ signaling genes in fibroblastic tumors. As a poor prognostic marker, fibroblastic TMEs were associated with significantly worse PFS ($p = 0.016$) with a trend towards worse OS ($p = 0.057$).

Cancer-associated fibroblasts and the dysregulation of endothelial cells have been shown to exert immunosuppressive effects in the TME through multiple mechanisms [86-88]. Cancer-associated fibroblasts can secrete a number of soluble factors (e.g. TGF- β , GAS6, GDF15, and FGF5) that can increase the aggressivity and metastatic potential of malignant cells [87, 89, 90]. Metastatic potential of tumor cells is further increased through disruption and remodeling of the extracellular matrix by cancer-associated fibroblasts [87, 89, 90]. Fibroblasts can also secrete VEGF and other cytokines/chemokines (e.g. TGF- β , IL-6, CXCL9) that interfere with effector leukocyte function, primarily cytotoxic T cell response [87, 91, 92]. Lastly, dysregulation of immune cells can occur through depletion of amino acids and lactate shuffling as a consequence of altered metabolic pathways between tumor cells and cancer-associated fibroblasts [87, 93, 94].

Tumor endothelial cells can impact the immune cell population in the TME through several mechanisms. First, endothelial cells guide immune cells into the tumor stroma via chemokines (e.g. CXCL4), integrins, and other adhesion molecules [88]. Increased secretion of factors (e.g. VEGF or FGF2) by tumor cells can result abnormal endothelial cell and vasculature, leading to downregulation of essential adhesion molecules and poor infiltration of leukocytes into the TME [88, 95-97]. Next, tumor

endothelial cells may also express inhibitory molecules that suppress effector cytotoxic T cell function and infiltration (e.g. PD-L1, Fas-ligand) [88, 98, 99]. Furthermore, an abnormal vascular network from tumor endothelial cells results in defective, leaky vessels which increase metastatic potential and also tumor hypoxia, resulting in further propagation of neoangiogenesis and the immunosuppressive effects of VEGF [100-102].

Selection of an adjunctive agent that can combat the immunosuppressive and deleterious effects of cancer-associated fibroblasts and endothelial cells may overcome pembrolizumab and other PD-1 inhibitor resistance in MSI-H endometrial tumors. For endothelial cells and dysregulated angiogenesis, combination with anti-VEGF agents such as bevacizumab (anti-VEGF monoclonal antibody) or oral tyrosine kinase inhibitors with anti-angiogenic effects may be useful. In a phase II trial, pembrolizumab with lenvatinib (multi-tyrosine kinase inhibitor with anti-VEGFR1-3 activity) was demonstrated to have great response rates in MSI-H endometrial tumors (ORR 63.6%; 7 of 11) [103]. However, it remains to be determined whether the addition of lenvatinib overcomes innate PD-1 resistance in MSI-H endometrial cancer. For cancer-associated fibroblasts, inhibitors of fibroblast activation (e.g. FGFR inhibitor) and/or action (TGF- β inhibitor) may prove beneficial and should be evaluated in pre-clinical studies and subsequent clinical trials.

Strengths on this thesis include that there are few studies in the literature that have focused on dissecting the intricacies of immuno-genomic profiles within MSI-H endometrial TMEs. Furthermore, this data correlates transcriptomic and mIF panel testing with response to treatment to pembrolizumab. However, there are several limitations. The small sample size prevent any definitive conclusions from being drawn

regarding predictive biomarkers of response to pembrolizumab and this also may have limited the power to detect statistically significant differences in the cancer-associated fibroblast panel testing. Furthermore, although the response rate to PD-1 inhibitors is approximately 50%, this cohort had a higher proportion of responders compared to non-responders (66.7% vs 33.3%) and this further limits the power to detect differences between groups.

This thesis provides an exciting early signal into biomarkers of resistance to pembrolizumab in MSI-H endometrial tumors. However, future studies will be needed to confirm the transcriptomic findings observed. Utilizing the current sample set, MIF panel analysis will be performed utilizing exploratory biomarkers for cancer-associated fibroblasts (α -SMA, Thy-1, S-100, FAP). Additionally, imaging mass cytometry will be performed using a broad panel of immune and non-immune cell markers (including markers for endothelial cells and fibroblasts). Future validation studies include repeating the transcriptomic profiling of tumors with MIF panel and imaging mass cytometry correlative studies from an independent cohort of MSI-H endometrial cancer patients treated with pembrolizumab. Additionally, transcriptomic profiling may be performed using an animal model such as the mouse model of MSI-H endometrial cancer developed by Dr. Melinda Yates and colleagues at MD Anderson. In this mouse model, MSH2 gene knockout will be achieved using the using progesterone receptor-Cre recombinase. By 12 months of age, approximately 40% of these mice with MSH2 gene knockout will develop complex atypical hyperplasia or endometrial cancer; all tumors are MSI-H. These mice with endometrial cancer will be treated with pembrolizumab and identification of responders and non-responders will be identified. Pre-treatment and post-treatment tumor samples from responders and non-responders

will be analyzed using RNA-seq and biomarker panel testing in order to evaluate whether fibroblasts and endothelial cells in the TME impact response to treatment.

Conclusions

In summary, there is great heterogeneity in the TME observed within patients with MSI-H endometrial cancer. Endometrial TME subtype may be an important prognosticator in the era of immunotherapy and may also play an integral part in shaping response to pembrolizumab monotherapy. Enrichment of endothelial cells and fibroblasts in the TME may be a predictive biomarker for poor response to pembrolizumab and should be evaluated in future validation studies. [4]

Bibliography

1. Siegel RL, Miller KD, Fuchs HE, Jemal A. Cancer Statistics, 2021. *CA Cancer J Clin.* 2021;71(1):7-33.
2. Bokhman JV. Two pathogenetic types of endometrial carcinoma. *Gynecol Oncol.* 1983;15(1):10-7.
3. Felix AS, Weissfeld JL, Stone RA, Bowser R, Chivukula M, Edwards RP, Linkov F. Factors associated with Type I and Type II endometrial cancer. *Cancer Causes Control.* 2010;21(11):1851-6.
4. Lu KH, Broaddus RR. Endometrial Cancer. *New England Journal of Medicine.* 2020;383(21):2053-64.
5. Doll A, Abal M, Rigau M, Monge M, Gonzalez M, Demajo S, Colás E, Llauradó M, Alazzouzi H, Planagumá J, Lohmann MA, Garcia J, Castellvi S, Ramon y Cajal J, Gil-Moreno A, Xercavins J, Alameda F, Reventós J. Novel molecular profiles of endometrial cancer-new light through old windows. *J Steroid Biochem Mol Biol.* 2008;108(3-5):221-9.
6. Setiawan VW, Yang HP, Pike MC, McCann SE, Yu H, Xiang YB, Wolk A, Wentzensen N, Weiss NS, Webb PM, van den Brandt PA, van de Vijver K, Thompson PJ, Strom BL, Spurdle AB, Soslow RA, Shu XO, Schairer C, Sacerdote C, Rohan TE, Robien K, Risch HA, Ricceri F, Rebbeck TR, Rastogi R, Prescott J, Polidoro S, Park Y, Olson SH, Moysich KB, Miller AB, McCullough ML, Matsuno RK, Magliocco AM, Lurie G, Lu L, Lissowska J, Liang X, Lacey JV, Jr., Kolonel LN, Henderson BE, Hankinson SE, Håkansson N, Goodman MT, Gaudet MM, Garcia-Closas M, Friedenreich CM, Freudenheim JL, Doherty J, De Vivo I, Courneya KS, Cook LS, Chen C, Cerhan JR, Cai H, Brinton LA, Bernstein L, Anderson KE, Anton-Culver H, Schouten LJ, Horn-Ross

PL. Type I and II endometrial cancers: have they different risk factors? J Clin Oncol. 2013;31(20):2607-18.

7. Saed L, Varse F, Baradaran HR, Moradi Y, Khateri S, Friberg E, Khazaei Z, Gharahjeh S, Tehrani S, Sioofy-Khojine AB, Najmi Z. The effect of diabetes on the risk of endometrial Cancer: an updated a systematic review and meta-analysis. BMC Cancer. 2019;19(1):527.
8. Barry JA, Azizia MM, Hardiman PJ. Risk of endometrial, ovarian and breast cancer in women with polycystic ovary syndrome: a systematic review and meta-analysis. Hum Reprod Update. 2014;20(5):748-58.
9. Lewin SN, Herzog TJ, Medel NIB, Deutsch I, Burke WM, Sun X, Wright JD. Comparative Performance of the 2009 International Federation of Gynecology and Obstetrics' Staging System for Uterine Corpus Cancer. Obstetrics & Gynecology. 2010;116(5).
10. Dellinger TH, Monk BJ. Systemic therapy for recurrent endometrial cancer: a review of North American trials. Expert Rev Anticancer Ther. 2009;9(7):905-16.
11. Dizon DS. Treatment options for advanced endometrial carcinoma. Gynecol Oncol. 2010;117(2):373-81.
12. Muggia FM, Blessing JA, Sorosky J, Reid GC. Phase II trial of the pegylated liposomal doxorubicin in previously treated metastatic endometrial cancer: a Gynecologic Oncology Group study. J Clin Oncol. 2002;20(9):2360-4.
13. Dizon DS, Blessing JA, McMeekin DS, Sharma SK, Disilvestro P, Alvarez RD. Phase II trial of ixabepilone as second-line treatment in advanced endometrial cancer: gynecologic oncology group trial 129-P. J Clin Oncol. 2009;27(19):3104-8.

14. Aghajanian C, Sill MW, Darcy KM, Greer B, McMeekin DS, Rose PG, Rotmensch J, Barnes MN, Hanjani P, Leslie KK. Phase II trial of bevacizumab in recurrent or persistent endometrial cancer: a Gynecologic Oncology Group study. *J Clin Oncol*. 2011;29(16):2259-65.
15. Alvarez EA, Brady WE, Walker JL, Rotmensch J, Zhou XC, Kendrick JE, Yamada SD, Schilder JM, Cohn DE, Harrison CR, Moore KN, Aghajanian C. Phase II trial of combination bevacizumab and temsirolimus in the treatment of recurrent or persistent endometrial carcinoma: a Gynecologic Oncology Group study. *Gynecol Oncol*. 2013;129(1):22-7.
16. Kandoth C, Schultz N, Cherniack AD, Akbani R, Liu Y, Shen H, Robertson AG, Pashtan I, Shen R, Benz CC, Yau C, Laird PW, Ding L, Zhang W, Mills GB, Kucherlapati R, Mardis ER, Levine DA. Integrated genomic characterization of endometrial carcinoma. *Nature*. 2013;497(7447):67-73.
17. Pećina-Šlaus N, Kafka A, Salamon I, Bukovac A. Mismatch Repair Pathway, Genome Stability and Cancer. *Front Mol Biosci*. 2020;7:122.
18. Murali R, Soslow RA, Weigelt B. Classification of endometrial carcinoma: more than two types. *Lancet Oncol*. 2014;15(7):e268-78.
19. Karamurzin Y, Rutgers JK. DNA mismatch repair deficiency in endometrial carcinoma. *Int J Gynecol Pathol*. 2009;28(3):239-55.
20. van den Heerik A, Horeweg N, de Boer SM, Bosse T, Creutzberg CL. Adjuvant therapy for endometrial cancer in the era of molecular classification: radiotherapy, chemoradiation and novel targets for therapy. *Int J Gynecol Cancer*. 2021;31(4):594-604.

21. León-Castillo A, de Boer SM, Powell ME, Mileschkin LR, Mackay HJ, Leary A, Nijman HW, Singh N, Pollock PM, Bessette P, Fyles A, Haie-Meder C, Smit V, Edmondson RJ, Putter H, Kitchener HC, Crosbie EJ, de Bruyn M, Nout RA, Horeweg N, Creutzberg CL, Bosse T. Molecular Classification of the PORTEC-3 Trial for High-Risk Endometrial Cancer: Impact on Prognosis and Benefit From Adjuvant Therapy. *J Clin Oncol*. 2020;38(29):3388-97.
22. Le DT, Durham JN, Smith KN, Wang H, Bartlett BR, Aulakh LK, Lu S, Kemberling H, Wilt C, Luber BS, Wong F, Azad NS, Rucki AA, Laheru D, Donehower R, Zaheer A, Fisher GA, Crocenzi TS, Lee JJ, Greten TF, Duffy AG, Ciombor KK, Eyring AD, Lam BH, Joe A, Kang SP, Holdhoff M, Danilova L, Cope L, Meyer C, Zhou S, Goldberg RM, Armstrong DK, Bever KM, Fader AN, Taube J, Housseau F, Spetzler D, Xiao N, Pardoll DM, Papadopoulos N, Kinzler KW, Eshleman JR, Vogelstein B, Anders RA, Diaz LA, Jr. Mismatch repair deficiency predicts response of solid tumors to PD-1 blockade. *Science (New York, NY)*. 2017;357(6349):409-13.
23. Koebel CM, Vermi W, Swann JB, Zerafa N, Rodig SJ, Old LJ, Smyth MJ, Schreiber RD. Adaptive immunity maintains occult cancer in an equilibrium state. *Nature*. 2007;450(7171):903-7.
24. Freeman GJ, Long AJ, Iwai Y, Bourque K, Chernova T, Nishimura H, Fitz LJ, Malenkovich N, Okazaki T, Byrne MC, Horton HF, Fouser L, Carter L, Ling V, Bowman MR, Carreno BM, Collins M, Wood CR, Honjo T. Engagement of the PD-1 immunoinhibitory receptor by a novel B7 family member leads to negative regulation of lymphocyte activation. *J Exp Med*. 2000;192(7):1027-34.
25. Okazaki T, Honjo T. PD-1 and PD-1 ligands: from discovery to clinical application. *Int Immunol*. 2007;19(7):813-24.

26. Levinson K, Dorigo O, Rubin K, Moore K. Immunotherapy in Gynecologic Cancers: What We Know Now and Where We Are Headed. American Society of Clinical Oncology Educational Book. 2019(39):e126-e40.
27. Pardoll DM. The blockade of immune checkpoints in cancer immunotherapy. *Nat Rev Cancer*. 2012;12(4):252-64.
28. Le DT, Uram JN, Wang H, Bartlett BR, Kemberling H, Eyring AD, Skora AD, Lubner BS, Azad NS, Laheru D, Biedrzycki B, Donehower RC, Zaheer A, Fisher GA, Crocenzi TS, Lee JJ, Duffy SM, Goldberg RM, de la Chapelle A, Koshiji M, Bhaijee F, Huebner T, Hruban RH, Wood LD, Cuka N, Pardoll DM, Papadopoulos N, Kinzler KW, Zhou S, Cornish TC, Taube JM, Anders RA, Eshleman JR, Vogelstein B, Diaz LA, Jr. PD-1 Blockade in Tumors with Mismatch-Repair Deficiency. *N Engl J Med*. 2015;372(26):2509-20.
29. Marabelle A, Le DT, Ascierto PA, Di Giacomo AM, De Jesus-Acosta A, Delord J-P, Geva R, Gottfried M, Penel N, Hansen AR, Piha-Paul SA, Doi T, Gao B, Chung HC, Lopez-Martin J, Bang Y-J, Frommer RS, Shah M, Ghorri R, Joe AK, Pruitt SK, Diaz Jr LA. Efficacy of Pembrolizumab in Patients With Noncolorectal High Microsatellite Instability/Mismatch Repair–Deficient Cancer: Results From the Phase II KEYNOTE-158 Study. *Journal of Clinical Oncology*. 2019;38(1):1-10.
30. Ott PA, Bang YJ, Berton-Rigaud D, Elez E, Pishvaian MJ, Rugo HS, Puzanov I, Mehnert JM, Aung KL, Lopez J, Carrigan M, Saraf S, Chen M, Soria JC. Safety and Antitumor Activity of Pembrolizumab in Advanced Programmed Death Ligand 1-Positive Endometrial Cancer: Results From the KEYNOTE-028 Study. *J Clin Oncol*. 2017;35(22):2535-41.

31. Oaknin A, Tinker AV, Gilbert L, Samouëlian V, Mathews C, Brown J, Barretina-Ginesta MP, Moreno V, Gravina A, Abdeddaim C, Banerjee S, Guo W, Danaee H, Im E, Sabatier R. Clinical Activity and Safety of the Anti-Programmed Death 1 Monoclonal Antibody Dostarlimab for Patients With Recurrent or Advanced Mismatch Repair-Deficient Endometrial Cancer: A Nonrandomized Phase 1 Clinical Trial. *JAMA Oncol.* 2020;6(11):1-7.
32. Konstantinopoulos PA, Luo W, Liu JF, Gulhan DC, Krasner C, Ishizuka JJ, Gockley AA, Buss M, Growdon WB, Crowe H, Campos S, Lindeman NI, Hill S, Stover E, Schumer S, Wright AA, Curtis J, Quinn R, Whalen C, Gray KP, Penson RT, Cannistra SA, Fleming GF, Matulonis UA. Phase II Study of Avelumab in Patients With Mismatch Repair Deficient and Mismatch Repair Proficient Recurrent/Persistent Endometrial Cancer. *J Clin Oncol.* 2019;37(30):2786-94.
33. Azad NS, Gray RJ, Overman MJ, Schoenfeld JD, Mitchell EP, Zwiebel JA, Sharon E, Streicher H, Li S, McShane LM, Rubinstein L, Patton DR, Williams PM, Coffey B, Hamilton SR, Bahary N, Suga JM, Hatoum H, Abrams JS, Conley BA, Arteaga CL, Harris L, O'Dwyer PJ, Chen AP, Flaherty KT. Nivolumab Is Effective in Mismatch Repair-Deficient Noncolorectal Cancers: Results From Arm Z1D-A Subprotocol of the NCI-MATCH (EAY131) Study. *J Clin Oncol.* 2020;38(3):214-22.
34. Antill YC, Kok PS, Robledo K, Barnes E, Friedlander M, Baron-Hay SE, Shannon CM, Coward J, Beale PJ, Goss G, Meniawy T, Yip S, Smith D, Spurdle AB, Parry M, Andrews J, Kelly M, Stockler MR, Mileskin LR. Activity of durvalumab in advanced endometrial cancer (AEC) according to mismatch repair (MMR) status: The phase II PHAEDRA trial (ANZGOG1601). *Journal of Clinical Oncology.* 2019;37(15_suppl):5501-.

35. Thompson JA, Schneider BJ, Brahmer J, Andrews S, Armand P, Bhatia S, Budde LE, Costa L, Davies M, Dunnington D, Ernstoff MS, Frigault M, Hoffner B, Hoimes CJ, Lacouture M, Locke F, Lunning M, Mohindra NA, Naidoo J, Olszanski AJ, Oluwole O, Patel SP, Reddy S, Ryder M, Santomasso B, Shofer S, Sosman JA, Wahidi M, Wang Y, Johnson-Chilla A, Scavone JL. Management of Immunotherapy-Related Toxicities, Version 1.2019. *J Natl Compr Canc Netw*. 2019;17(3):255-89.
36. Pauken KE, Sammons MA, Odorizzi PM, Manne S, Godec J, Khan O, Drake AM, Chen Z, Sen DR, Kurachi M, Barnitz RA, Bartman C, Bengsch B, Huang AC, Schenkel JM, Vahedi G, Haining WN, Berger SL, Wherry EJ. Epigenetic stability of exhausted T cells limits durability of reinvigoration by PD-1 blockade. *Science*. 2016;354(6316):1160-5.
37. Koyama S, Akbay EA, Li YY, Herter-Sprie GS, Buczkowski KA, Richards WG, Gandhi L, Redig AJ, Rodig SJ, Asahina H, Jones RE, Kulkarni MM, Kuraguchi M, Palakurthi S, Fecci PE, Johnson BE, Janne PA, Engelman JA, Gangadharan SP, Costa DB, Freeman GJ, Bueno R, Hodi FS, Dranoff G, Wong KK, Hammerman PS. Adaptive resistance to therapeutic PD-1 blockade is associated with upregulation of alternative immune checkpoints. *Nat Commun*. 2016;7:10501.
38. Anagnostou V, Smith KN, Forde PM, Niknafs N, Bhattacharya R, White J, Zhang T, Adleff V, Phallen J, Wali N, Hruban C, Guthrie VB, Rodgers K, Naidoo J, Kang H, Sharfman W, Georgiades C, Verde F, Illei P, Li QK, Gabrielson E, Brock MV, Zahnow CA, Baylin SB, Scharpf RB, Brahmer JR, Karchin R, Pardoll DM, Velculescu VE. Evolution of Neoantigen Landscape during Immune Checkpoint Blockade in Non-Small Cell Lung Cancer. *Cancer Discov*. 2017;7(3):264-76.

39. Zaretsky JM, Garcia-Diaz A, Shin DS, Escuin-Ordinas H, Hugo W, Hu-Lieskovan S, Torrejon DY, Abril-Rodriguez G, Sandoval S, Barthly L, Saco J, Homet Moreno B, Mezzadra R, Chmielowski B, Ruchalski K, Shintaku IP, Sanchez PJ, Puig-Saus C, Cherry G, Seja E, Kong X, Pang J, Berent-Maoz B, Comin-Anduix B, Graeber TG, Tumeh PC, Schumacher TN, Lo RS, Ribas A. Mutations Associated with Acquired Resistance to PD-1 Blockade in Melanoma. *N Engl J Med*. 2016;375(9):819-29.
40. Nowicki TS, Hu-Lieskovan S, Ribas A. Mechanisms of Resistance to PD-1 and PD-L1 Blockade. *Cancer J*. 2018;24(1):47-53.
41. Spranger S, Bao R, Gajewski TF. Melanoma-intrinsic β -catenin signalling prevents anti-tumour immunity. *Nature*. 2015;523(7559):231-5.
42. Loi S, Dushyanthen S, Beavis PA, Salgado R, Denkert C, Savas P, Combs S, Rimm DL, Giltane JM, Estrada MV, Sanchez V, Sanders ME, Cook RS, Pilkinton MA, Mallal SA, Wang K, Miller VA, Stephens PJ, Yelensky R, Doimi FD, Gomez H, Ryzhov SV, Darcy PK, Arteaga CL, Balko JM. RAS/MAPK Activation Is Associated with Reduced Tumor-Infiltrating Lymphocytes in Triple-Negative Breast Cancer: Therapeutic Cooperation Between MEK and PD-1/PD-L1 Immune Checkpoint Inhibitors. *Clin Cancer Res*. 2016;22(6):1499-509.
43. Liu C, Peng W, Xu C, Lou Y, Zhang M, Wargo JA, Chen JQ, Li HS, Watowich SS, Yang Y, Tompers Frederick D, Cooper ZA, Mbofung RM, Whittington M, Flaherty KT, Woodman SE, Davies MA, Radvanyi LG, Overwijk WW, Lizée G, Hwu P. BRAF inhibition increases tumor infiltration by T cells and enhances the antitumor activity of adoptive immunotherapy in mice. *Clin Cancer Res*. 2013;19(2):393-403.
44. Peng W, Chen JQ, Liu C, Malu S, Creasy C, Tetzlaff MT, Xu C, McKenzie JA, Zhang C, Liang X, Williams LJ, Deng W, Chen G, Mbofung R, Lazar AJ, Torres-Cabala

CA, Cooper ZA, Chen PL, Tieu TN, Spranger S, Yu X, Bernatchez C, Forget MA, Haymaker C, Amaria R, McQuade JL, Glitza IC, Cascone T, Li HS, Kwong LN, Heffernan TP, Hu J, Bassett RL, Jr., Bosenberg MW, Woodman SE, Overwijk WW, Lizee G, Roszik J, Gajewski TF, Wargo JA, Gershenwald JE, Radvanyi L, Davies MA, Hwu P. Loss of PTEN Promotes Resistance to T Cell-Mediated Immunotherapy. *Cancer Discov.* 2016;6(2):202-16.

45. Platanias LC. Mechanisms of type-I- and type-II-interferon-mediated signalling. *Nat Rev Immunol.* 2005;5(5):375-86.

46. Benci JL, Xu B, Qiu Y, Wu TJ, Dada H, Twyman-Saint Victor C, Cucolo L, Lee DSM, Pauken KE, Huang AC, Gangadhar TC, Amaravadi RK, Schuchter LM, Feldman MD, Ishwaran H, Vonderheide RH, Maity A, Wherry EJ, Minn AJ. Tumor Interferon Signaling Regulates a Multigenic Resistance Program to Immune Checkpoint Blockade. *Cell.* 2016;167(6):1540-54.e12.

47. Darnell JE, Jr., Kerr IM, Stark GR. Jak-STAT pathways and transcriptional activation in response to IFNs and other extracellular signaling proteins. *Science.* 1994;264(5164):1415-21.

48. Shin DS, Zaretsky JM, Escuin-Ordinas H, Garcia-Diaz A, Hu-Lieskovan S, Kalbasi A, Grasso CS, Hugo W, Sandoval S, Torrejon DY, Palaskas N, Rodriguez GA, Parisi G, Azhdam A, Chmielowski B, Cherry G, Seja E, Berent-Maoz B, Shintaku IP, Le DT, Pardoll DM, Diaz LA, Jr., Tumei PC, Graeber TG, Lo RS, Comin-Anduix B, Ribas A. Primary Resistance to PD-1 Blockade Mediated by JAK1/2 Mutations. *Cancer Discov.* 2017;7(2):188-201.

49. Manguso RT, Pope HW, Zimmer MD, Brown FD, Yates KB, Miller BC, Collins NB, Bi K, LaFleur MW, Juneja VR, Weiss SA, Lo J, Fisher DE, Miao D, Van Allen E,

Root DE, Sharpe AH, Doench JG, Haining WN. In vivo CRISPR screening identifies Ptpn2 as a cancer immunotherapy target. *Nature*. 2017;547(7664):413-8.

50. D'Urso CM, Wang ZG, Cao Y, Tatake R, Zeff RA, Ferrone S. Lack of HLA class I antigen expression by cultured melanoma cells FO-1 due to a defect in B2m gene expression. *J Clin Invest*. 1991;87(1):284-92.

51. Sucker A, Zhao F, Real B, Heeke C, Bielefeld N, Maßen S, Horn S, Moll I, Maltaner R, Horn PA, Schilling B, Sabbatino F, Lennerz V, Kloor M, Ferrone S, Schadendorf D, Falk CS, Griewank K, Paschen A. Genetic evolution of T-cell resistance in the course of melanoma progression. *Clin Cancer Res*. 2014;20(24):6593-604.

52. Chabanon RM, Pedrero M, Lefebvre C, Marabelle A, Soria JC, Postel-Vinay S. Mutational Landscape and Sensitivity to Immune Checkpoint Blockers. *Clin Cancer Res*. 2016;22(17):4309-21.

53. Samstein RM, Lee CH, Shoushtari AN, Hellmann MD, Shen R, Janjigian YY, Barron DA, Zehir A, Jordan EJ, Omuro A, Kaley TJ, Kendall SM, Motzer RJ, Hakimi AA, Voss MH, Russo P, Rosenberg J, Iyer G, Bochner BH, Bajorin DF, Al-Ahmadie HA, Chaft JE, Rudin CM, Riely GJ, Baxi S, Ho AL, Wong RJ, Pfister DG, Wolchok JD, Barker CA, Gutin PH, Brennan CW, Tabar V, Mellinghoff IK, DeAngelis LM, Ariyan CE, Lee N, Tap WD, Gounder MM, D'Angelo SP, Saltz L, Stadler ZK, Scher HI, Baselga J, Razavi P, Klebanoff CA, Yaeger R, Segal NH, Ku GY, DeMatteo RP, Ladanyi M, Rizvi NA, Berger MF, Riaz N, Solit DB, Chan TA, Morris LGT. Tumor mutational load predicts survival after immunotherapy across multiple cancer types. *Nat Genet*. 2019;51(2):202-6.

54. Goodman AM, Kato S, Bazhenova L, Patel SP, Frampton GM, Miller V, Stephens PJ, Daniels GA, Kurzrock R. Tumor Mutational Burden as an Independent Predictor of Response to Immunotherapy in Diverse Cancers. *Mol Cancer Ther*. 2017;16(11):2598-608.
55. Valero C, Lee M, Hoen D, Zehir A, Berger MF, Seshan VE, Chan TA, Morris LGT. Response Rates to Anti-PD-1 Immunotherapy in Microsatellite-Stable Solid Tumors With 10 or More Mutations per Megabase. *JAMA Oncol*. 2021.
56. Pollard JW. Tumour-educated macrophages promote tumour progression and metastasis. *Nat Rev Cancer*. 4. England2004. p. 71-8.
57. Binnewies M, Roberts EW, Kersten K, Chan V, Fearon DF, Merad M, Coussens LM, Gabrilovich DI, Ostrand-Rosenberg S, Hedrick CC, Vonderheide RH, Pittet MJ, Jain RK, Zou W, Howcroft TK, Woodhouse EC, Weinberg RA, Krummel MF. Understanding the tumor immune microenvironment (TIME) for effective therapy. *Nat Med*. 2018;24(5):541-50.
58. Gabrilovich DI, Nagaraj S. Myeloid-derived suppressor cells as regulators of the immune system. *Nat Rev Immunol*. 2009;9(3):162-74.
59. Ostrand-Rosenberg S. Myeloid-derived suppressor cells: more mechanisms for inhibiting antitumor immunity. *Cancer Immunol Immunother*. 2010;59(10):1593-600.
60. Highfill SL, Cui Y, Giles AJ, Smith JP, Zhang H, Morse E, Kaplan RN, Mackall CL. Disruption of CXCR2-mediated MDSC tumor trafficking enhances anti-PD1 efficacy. *Sci Transl Med*. 2014;6(237):237ra67.
61. Eggink FA, Van Gool IC, Leary A, Pollock PM, Crosbie EJ, Mileskin L, Jordanova ES, Adam J, Freeman-Mills L, Church DN, Creutzberg CL, De Bruyn M, Nijman HW, Bosse T. Immunological profiling of molecularly classified high-risk

endometrial cancers identifies POLE-mutant and microsatellite unstable carcinomas as candidates for checkpoint inhibition. *Oncoimmunology*. 2017;6(2):e1264565.

62. Vilar E, Mork ME, Cuddy A, Borrás E, Bannon SA, Taggart MW, Ying J, Broaddus RR, Luthra R, Rodriguez-Bigas MA, Lynch PM, You YQ. Role of microsatellite instability-low as a diagnostic biomarker of Lynch syndrome in colorectal cancer. *Cancer Genet*. 2014;207(10-12):495-502.

63. Zhang L. Immunohistochemistry versus microsatellite instability testing for screening colorectal cancer patients at risk for hereditary nonpolyposis colorectal cancer syndrome. Part II. The utility of microsatellite instability testing. *J Mol Diagn*. 2008;10(4):301-7.

64. Wang R, Song S, Harada K, Ghazanfari Amlashi F, Badgwell B, Pizzi MP, Xu Y, Zhao W, Dong X, Jin J, Wang Y, Scott A, Ma L, Huo L, Vicente D, Blum Murphy M, Shanbhag N, Tatlonghari G, Thomas I, Rogers J, Kobayashi M, Vykoukal J, Estrella JS, Roy-Chowdhuri S, Han G, Zhang S, Mao X, Song X, Zhang J, Gu J, Johnson RL, Calin GA, Peng G, Lee JS, Hanash SM, Futreal A, Wang Z, Wang L, Ajani JA. Multiplex profiling of peritoneal metastases from gastric adenocarcinoma identified novel targets and molecular subtypes that predict treatment response. *Gut*. 2020;69(1):18-31.

65. Andrews S. FastQC: A Quality Control Tool for High Throughput Sequence Data 2010. Available from: <http://www.bioinformatics.babraham.ac.uk/projects/fastqc/>.

66. DeLuca DS, Levin JZ, Sivachenko A, Fennell T, Nazaire MD, Williams C, Reich M, Winckler W, Getz G. RNA-SeQC: RNA-seq metrics for quality control and process optimization. *Bioinformatics*. 2012;28(11):1530-2.

67. Dobin A, Davis CA, Schlesinger F, Drenkow J, Zaleski C, Jha S, Batut P, Chaisson M, Gingeras TR. STAR: ultrafast universal RNA-seq aligner. *Bioinformatics*. 2013;29(1):15-21.
68. Anders S, Pyl PT, Huber W. HTSeq--a Python framework to work with high-throughput sequencing data. *Bioinformatics*. 2015;31(2):166-9.
69. Love MI, Anders S, Kim V, Huber W. RNA-Seq workflow: gene-level exploratory analysis and differential expression. *F1000Res*. 2015;4:1070.
70. GDC N. RNA-seq quantification. Available from: <https://gdc.cancer.gov/about-data/data-harmonization-and-generation/genomic-data-harmonization/high-level-data-generation/rna-seq-quantification>.
71. Commons NCIGD. RNA-seq quantification. Available from: <https://gdc.cancer.gov/about-data/data-harmonization-and-generation/genomic-data-harmonization/high-level-data-generation/rna-seq-quantification>.
72. Becht E, Giraldo NA, Lacroix L, Buttard B, Elarouci N, Petitprez F, Selves J, Laurent-Puig P, Sautès-Fridman C, Fridman WH, de Reyniès A. Estimating the population abundance of tissue-infiltrating immune and stromal cell populations using gene expression. *Genome Biol*. 2016;17(1):218.
73. Parra ER, Uraoka N, Jiang M, Cook P, Gibbons D, Forget MA, Bernatchez C, Haymaker C, Wistuba, II, Rodriguez-Canales J. Validation of multiplex immunofluorescence panels using multispectral microscopy for immune-profiling of formalin-fixed and paraffin-embedded human tumor tissues. *Sci Rep*. 2017;7(1):13380.
74. Parra ER, Francisco-Cruz A, Wistuba, II. State-of-the-Art of Profiling Immune Contexture in the Era of Multiplexed Staining and Digital Analysis to Study Paraffin Tumor Tissues. *Cancers (Basel)*. 2019;11(2).

75. Parra ER, Jiang M, Solis L, Mino B, Laberiano C, Hernandez S, Gite S, Verma A, Tetzlaff M, Haymaker C, Tamegnon A, Rodriguez-Canales J, Hoyd C, Bernachez C, Wistuba I. Procedural Requirements and Recommendations for Multiplex Immunofluorescence Tyramide Signal Amplification Assays to Support Translational Oncology Studies. *Cancers (Basel)*. 2020;12(2).
76. Taube JM, Akturk G, Angelo M, Engle EL, Gnjatic S, Greenbaum S, Greenwald NF, Hedvat CV, Hollmann TJ, Juco J, Parra ER, Rebelatto MC, Rimm DL, Rodriguez-Canales J, Schalper KA, Stack EC, Ferreira CS, Korski K, Lako A, Rodig SJ, Schenck E, Steele KE, Surace MJ, Tetzlaff MT, von Loga K, Wistuba, II, Bifulco CB. The Society for Immunotherapy of Cancer statement on best practices for multiplex immunohistochemistry (IHC) and immunofluorescence (IF) staining and validation. *J Immunother Cancer*. 2020;8(1).
77. Stack EC, Wang C, Roman KA, Hoyt CC. Multiplexed immunohistochemistry, imaging, and quantitation: a review, with an assessment of Tyramide signal amplification, multispectral imaging and multiplex analysis. *Methods*. 2014;70(1):46-58.
78. Benjamini Y, Drai D, Elmer G, Kafkafi N, Golani I. Controlling the false discovery rate in behavior genetics research. *Behav Brain Res*. 2001;125(1-2):279-84.
79. Li BL, Wan XP. Prognostic significance of immune landscape in tumour microenvironment of endometrial cancer. *J Cell Mol Med*. 2020;24(14):7767-77.
80. Wang G, Wang D, Sun M, Liu X, Yang Q. Identification of prognostic and immune-related gene signatures in the tumor microenvironment of endometrial cancer. *Int Immunopharmacol*. 2020;88:106931.
81. Pakish JB, Zhang Q, Chen Z, Liang H, Chisholm GB, Yuan Y, Mok SC, Broaddus RR, Lu KH, Yates MS. Immune Microenvironment in Microsatellite-Unstable

Endometrial Cancers: Hereditary or Sporadic Origin Matters. *Clin Cancer Res.* 2017;23(15):4473-81.

82. Dun EC, Hanley K, Wieser F, Bohman S, Yu J, Taylor RN. Infiltration of tumor-associated macrophages is increased in the epithelial and stromal compartments of endometrial carcinomas. *Int J Gynecol Pathol.* 2013;32(6):576-84.

83. Kübler K, Ayub TH, Weber SK, Zivanovic O, Abramian A, Keyver-Paik MD, Mallmann MR, Kaiser C, Serçe NB, Kuhn W, Rudlowski C. Prognostic significance of tumor-associated macrophages in endometrial adenocarcinoma. *Gynecol Oncol.* 2014;135(2):176-83.

84. Zhan L, Liu X, Zhang J, Cao Y, Wei B. Immune disorder in endometrial cancer: Immunosuppressive microenvironment, mechanisms of immune evasion and immunotherapy. *Oncol Lett.* 2020;20(3):2075-90.

85. Liu Y, Zugazagoitia J, Ahmed FS, Henick BS, Gettinger SN, Herbst RS, Schalper KA, Rimm DL. Immune Cell PD-L1 Colocalizes with Macrophages and Is Associated with Outcome in PD-1 Pathway Blockade Therapy. *Clin Cancer Res.* 2020;26(4):970-7.

86. Han C, Liu T, Yin R. Biomarkers for cancer-associated fibroblasts. *Biomark Res.* 2020;8(1):64.

87. Sahai E, Astsaturov I, Cukierman E, DeNardo DG, Egeblad M, Evans RM, Fearon D, Greten FR, Hingorani SR, Hunter T, Hynes RO, Jain RK, Janowitz T, Jorgensen C, Kimmelman AC, Kolonin MG, Maki RG, Powers RS, Puré E, Ramirez DC, Scherz-Shouval R, Sherman MH, Stewart S, Tlsty TD, Tuveson DA, Watt FM, Weaver V, Weeraratna AT, Werb Z. A framework for advancing our understanding of cancer-associated fibroblasts. *Nat Rev Cancer.* 2020;20(3):174-86.

88. Nagl L, Horvath L, Pircher A, Wolf D. Tumor Endothelial Cells (TECs) as Potential Immune Directors of the Tumor Microenvironment - New Findings and Future Perspectives. *Front Cell Dev Biol.* 2020;8:766.
89. Liu T, Han C, Wang S, Fang P, Ma Z, Xu L, Yin R. Cancer-associated fibroblasts: an emerging target of anti-cancer immunotherapy. *J Hematol Oncol.* 2019;12(1):86.
90. Shiga K, Hara M, Nagasaki T, Sato T, Takahashi H, Takeyama H. Cancer-Associated Fibroblasts: Their Characteristics and Their Roles in Tumor Growth. *Cancers (Basel).* 2015;7(4):2443-58.
91. Monteran L, Erez N. The Dark Side of Fibroblasts: Cancer-Associated Fibroblasts as Mediators of Immunosuppression in the Tumor Microenvironment. *Front Immunol.* 2019;10:1835.
92. Fearon DT. The carcinoma-associated fibroblast expressing fibroblast activation protein and escape from immune surveillance. *Cancer Immunol Res.* 2014;2(3):187-93.
93. Bertero T, Oldham WM, Grasset EM, Bourget I, Boulter E, Pisano S, Hofman P, Bellvert F, Meneguzzi G, Bulavin DV, Estrach S, Feral CC, Chan SY, Bozec A, Gaggioli C. Tumor-Stroma Mechanics Coordinate Amino Acid Availability to Sustain Tumor Growth and Malignancy. *Cell Metab.* 2019;29(1):124-40.e10.
94. Sanford-Crane H, Abrego J, Sherman MH. Fibroblasts as Modulators of Local and Systemic Cancer Metabolism. *Cancers (Basel).* 2019;11(5).
95. Griffioen AW, Damen CA, Mayo KH, Barendsz-Janson AF, Martinotti S, Blijham GH, Groenewegen G. Angiogenesis inhibitors overcome tumor induced endothelial cell anergy. *Int J Cancer.* 1999;80(2):315-9.

96. Flati V, Pastore LI, Griffioen AW, Satijn S, Toniato E, D'Alimonte I, Laglia E, Marchetti P, Gulino A, Martinotti S. Endothelial cell anergy is mediated by bFGF through the sustained activation of p38-MAPK and NF-kappaB inhibition. *Int J Immunopathol Pharmacol*. 2006;19(4):761-73.
97. Dirx AE, Oude Egbrink MG, Kuijpers MJ, van der Niet ST, Heijnen VV, Bouma-ter Steege JC, Wagstaff J, Griffioen AW. Tumor angiogenesis modulates leukocyte-vessel wall interactions in vivo by reducing endothelial adhesion molecule expression. *Cancer Res*. 2003;63(9):2322-9.
98. Georganaki M, van Hooren L, Dimberg A. Vascular Targeting to Increase the Efficiency of Immune Checkpoint Blockade in Cancer. *Front Immunol*. 2018;9:3081.
99. Motz GT, Santoro SP, Wang LP, Garrabrant T, Lastra RR, Hagemann IS, Lal P, Feldman MD, Benencia F, Coukos G. Tumor endothelium FasL establishes a selective immune barrier promoting tolerance in tumors. *Nat Med*. 2014;20(6):607-15.
100. Maishi N, Annan DA, Kikuchi H, Hida Y, Hida K. Tumor Endothelial Heterogeneity in Cancer Progression. *Cancers (Basel)*. 2019;11(10).
101. Butler JM, Kobayashi H, Rafii S. Instructive role of the vascular niche in promoting tumour growth and tissue repair by angiocrine factors. *Nat Rev Cancer*. 2020. p. 138-46.
102. De Palma M, Biziato D, Petrova TV. Microenvironmental regulation of tumour angiogenesis. *Nat Rev Cancer*. 2017;17(8):457-74.
103. Makker V, Taylor MH, Aghajanian C, Oaknin A, Mier J, Cohn AL, Romeo M, Bratos R, Brose MS, DiSimone C, Messing M, Stepan DE, Dutcus CE, Wu J, Schmidt EV, Orlowski R, Sachdev P, Shumaker R, Casado Herraiz A. Lenvatinib Plus

Pembrolizumab in Patients With Advanced Endometrial Cancer. J Clin Oncol.
2020;Jco1902627.

Vita

Jeffrey Andrew How was born in Montreal, Canada, the first son to Redge and Florence How. He grew up in Phoenix, Arizona and graduated from Desert Vista high school in 2007. He moved to back to his birth city where he completed a Diploma in College Studies in Health Sciences at Marianopolis College in 2009. Subsequently, he received his medical degree in 2014 from McGill University in Montreal, Canada. He continued his medical training at McGill and completed a 5-year residency in Obstetrics and Gynecology in 2019. In Canada, he is board-certified in Obstetrics and Gynecology and currently a Fellow of the Royal College of Surgeons of Canada. During his residency, he completed a part-time Master of Public Health at the Harvard T.H. Chan School of Public Health in Cambridge, Massachusetts in 2015. In August 2019, he entered The University of Texas MD Anderson Cancer Center UTHealth Graduate School of Biomedical Sciences. He is currently a Gynecologic Oncology Fellow at the University of Texas MD Anderson Cancer Center and will complete his training in June 2023.

Permanent address:

5927 Almeda Rd, unit 21006

Houston, Texas 77004